



**UNIVERSITY „POLITEHNICA” OF BUCHAREST
DOCTORAL SCHOOL OF ELECTRICAL ENGINEERING**

PHD THESIS SUMMARY

**ELECTROMECHANICAL INTERACTIONS IN THE SIZING AND
CONSTRUCTION OF DRIVING SYSTEMS WITH
MICROELECTROMECHANICAL INTEGRATION**

**INTERACȚIUNI ELECTROMECHANICE ÎN DIMENSIONAREA ȘI
CONSTRUCȚIA UNOR SISTEME DE ACȚIONARE CU INTEGRARE
MICROELECTROMECHANICĂ**

Author: Eng. Marius POPA

PhD supervisor: Prof. dr. eng. Alexandru Mihail MOREGA

**BUCUREȘTI
2021**

CONTENTS

CONTENTS	2
INTRODUCTION	3
CHAPTER 1 MAGNETOSTRICTIVE ACTUATORS.....	4
1.1 MAGNETOSTRICTIVE MATERIALS.....	4
1.2 TERFENOL-D - MATERIAL PROPERTIES.....	5
1.3 LINEAR MAGNETOSTRICTIVE ACTUATOR	6
1.4 MAGNETOSTRICTIVE ACTUATOR WITH PLANAR COILS	7
1.5. MAGNETOSTRICTIVE ACTUATOR WITH CYLINDRICAL COILS	9
1.6. PRACTICAL REALIZATION OF LINEAR MAGNETOSTRICTIVE ACTUATORS	12
1.7. STRUCTURAL OPTIMIZATION (CONSTRUCTAL) OF THE MODEL, REALIZATION AND TESTING OF THE IMPROVED VARIANT. EXPERIMENTAL TESTS..	13
CHAPTER 2 ELECTROMECHANICAL ACTUATORS	20
CHAPTER 3 PIEZOELECTRIC ACTUATORS.....	25
CHAPTER 4 FLYBACK TRANSFORMER FOR ENVIRONMENTAL ENERGY HARVESTING CONVERTER.....	28
CHAPTER 5 MANUFACTURING TECHNOLOGIES USED TO MAKE ACTUATORS	32
5.1. COIL AND MICROCOIL TECHNOLOGIES	32
5.2 PERMANENT MAGNET PROCESSING TECHNOLOGIES	35
5.3. TECHNOLOGIES FOR MAKING MAGNETOSTRICTIVE AND PIEZOELECTRIC ACTUATORS.....	38
5.4. MECHANICAL PARTS PROCESSING TECHNOLOGIES THROUGH UNCONVENTIONAL TECHNOLOGIES	40
CONCLUSIONS, CONTRIBUTIONS, PROSPECTS.....	43
REFERENCES	46

Keywords:

actuator, electromechanic, drive, MEMS, magnetostrictive, Terfenol, planar coil, piezoelectric, transformer, environmental energy, flyback, manufacturing technology, numerical simulation, numerical methods, premagnetization, bias, unconventional technologies, EDM, meshing, waveform, constructive optimization, experimental testing, Peltier element, cantilever actuator, structural model, own frequencies, nanofluid, electrodeposition.

INTRODUCTION

Microelectromechanical systems (MEMS, acronym for Micro-Electro-Mechanical System) represent the integration of mechanical elements, sensors, actuators and related electronics on a common substrate, processed by microfabrication technologies. The beneficiary fields of MEMS applications are numerous: automotive industry, health, process control, aerospace and defense industry, energy / environment, industrial applications / safety equipment, education / research, etc. Consumer products are an important and rapidly expanding market for microsensors.

In this context, the study of electromechanical interactions in a series of drive systems containing microelectromechanical elements, with the identification of technological solutions for practical realization, is a topical issue, a topic analyzed in this paper entitled "*Electromechanical interactions in the sizing and construction of driving systems with microelectromechanical integration*".

The first chapter presents magnetostrictive actuators. General elements related to these actuators are presented, magnetostrictive materials with practical applications are analyzed, deepening the characteristics for Terfenol- D. Linear actuators are analyzed and then the analyzes for magnetostrictive actuators with planar coils and for those with cylindrical coils are customized. It presents the practical realization of a magnetostrictive actuator, testing, construction optimization and improvement of the initial solution.

The second chapter of the thesis is to analyze electromechanical actuators. Electromechanical actuators have been studied with the cantilever beam in several versions. Structural deformations were determined eigenmodes structural models using reduced due to the symmetry and complete models.

The third chapter of the thesis presents piezoelectric actuators. Based on the mathematical model, shows the deformation of a piezoelectric cylinder, structural deformations and distortions are analyzed eigenmodes associated with the stator.

The fourth chapter is dedicated to a flyback transformer for an environmental energy converter. A hybrid transformer, with ferrite and magnetic nanofluid, is presented, which starts from the mathematical model, follows the results of numerical simulations and presents details of practical realization and results from measurements, with the test scheme.

The fifth chapter aims at analyzing, selecting and optimizing the technological processes involved in the realization of the actuators presented in the previous chapters. Following are the technologies for processing permanent magnets, by EDM and by magnetic field deposition. For the realization of magnetostrictive and piezoelectric actuators, the technologies used in two concrete cases are presented. As a common element of many applications is presented the realization and control of the coupling elements applicable in the field of microsystems.

Finally the thesis presents general conclusions, original contributions and development prospects.

CHAPTER 1

MAGNETOSTRICTIVE ACTUATORS

The design and construction of action systems based on magnetostrictive effect is an area of interest both in Romania and in the world, interest arising from the large number of articles and communications.

Actuators made basically based on the properties of magnetostrictive the material Terfenol-D, using magnetic activation (bias magnetic) and mechanical stress (bias mechanical) for the operation in an area of deformation relative $\Delta L / L$ important to the desired loading (Fig. 1). These deformations can be approximated linearly over relatively wide domains of the relative elongation curve depending on the intensity of the magnetic field for the Terfenol-D material and thus have a variation proportional to the applied magnetic field.

1.1 Magnetostrictive materials

Magnetostriction is a property of ferromagnetic materials having as main effect the expansion (positive magnetostriction) or contraction (negative magnetostriction) of a core subjected to the action of a magnetic field oriented in the direction of deformation. The effect is manifested mainly in the direction of the magnetic field (longitudinal effect), the relative elongation $\Delta L / L$ showing a tendency of saturation.

The relative elongation $\Delta L / L$ to the variation of the magnetic field, called magnetostrictive coefficient λ , is measurable in most ferromagnetic materials but at usual temperatures the effect is reduced. By alloying with certain elements, a "giant" magnetostriction (GMM) can be achieved, under the action of small external magnetic fields. Alloys containing Fe, Dy and Tb, type $Tb_xDy_{1-x}Fe_2$ are used for practical applications, Terfenol-D (*Ter -terbium, fe-ferrum, nol-Naval Ordonance Laboratory and D -dysprosium*) with the formula $Tb_{0.3}Dy_{0.7}Fe_{1.9}$ being the most used magnetostrictive material.

Galfenol alloys have a moderate magnetostrictive coefficient ($\lambda \sim 350$ ppm) at low magnetic field intensities (8 kA / m), with very low hysteresis and small variations in magnetomechanical properties for temperatures between -20 and 80° C, Curie temperature of 675° C and good corrosion resistance, able to work in harsh environments. Magnetostrictive materials (Terfenol, Galfenol, Alfenol) are not manufactured industrially in the country, there are a small number of manufacturers of such materials worldwide.

1.2 Terfenol-D - material properties

Terphenol-D in the form of a bar provides an important expansion (positive magnetostriction), at magnetic field intensities of 50-200 kA / m, expansion influenced by the pretensioning (mechanical bias) applied according to the graph in fig. 1.1.

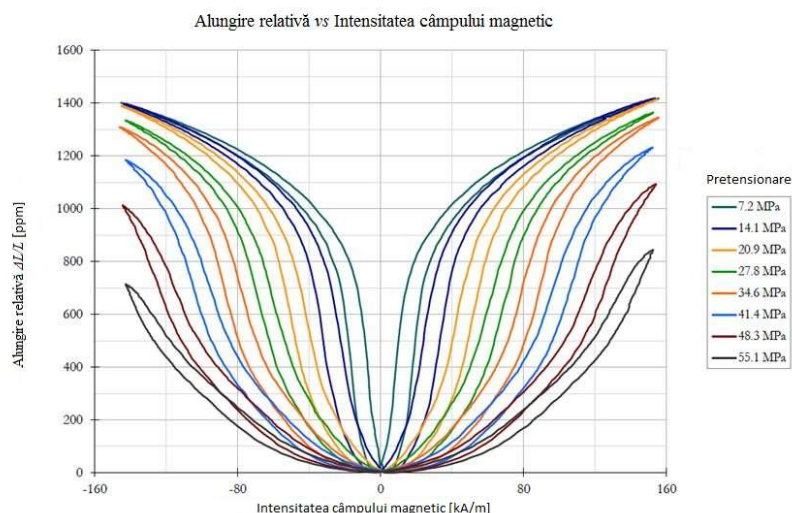


Figure 1.1 Variation of relative elongation depending on the intensity of the magnetic field, with various pretensions (mechanical bias)

By changing the concentrations of the component elements of Terfenol-D ($Tb_xDy_{1-x}Fe_{1.9...2}$), variants of Terfenol-D with different behaviors at low temperatures are obtained. Thus, the decrease of Terbium concentration leads to relatively low elongations for negative temperatures (fig. 1.2)

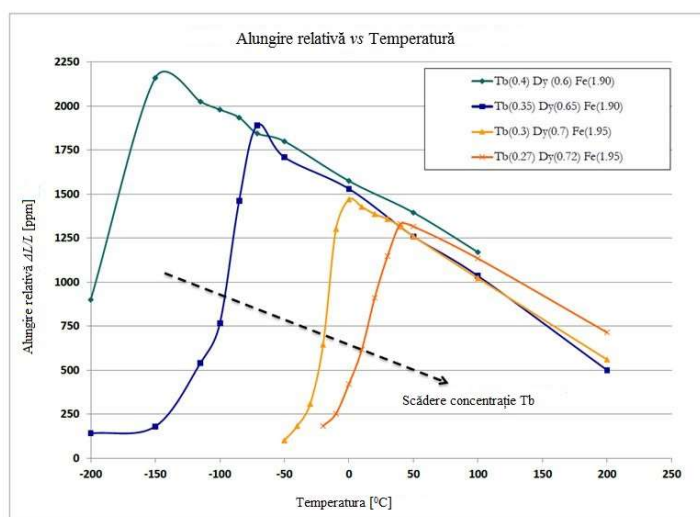


Figure 1.2 Variation of elongation relative to saturation as a function of temperature, for various variants of Terfenol-D

The magnetostrictive coefficient λ varies depending on the intensity of the magnetic field (for a fixed pre-tightening and premagnetization), existing on the variation curve $\Delta L / L$ depending on the intensity of the magnetic field (fig. 1.1) a region where the slope is high and the relationship between deformation and intensity the magnetic field is quasi-linear.

The activation field (bias) can be ensured by permanent magnets and / or a bias solenoid, the solution being chosen according to the specifics of the application.

Mechanical prestressing (mechanical bias - applied by means of an arc with known elastic constant) is chosen so as to obtain the desired deformations with a magnetic bias field intensity as low as possible.

1.3 Linear magnetostrictive actuator

In the literature are presented examples of magnetostrictive actuators that are at the level of experimental model, but there are numerous commercial products (Fig. 1.3) that certify the interest for such products.



Figure 1.3 Direct magnetostrictive actuator (DMA) and amplified magnetostrictive actuators (AMA) manufactured by Cedrat Technology

The direct magnetostrictive actuator produced by Cedrat Technologies called DMA 100L was created for applications that require high pressure. The magnetic bias field can be adjusted from 0 to 100 kA / m. Also the prestressing can be adjusted from 0 - 40Mpa.

The magnetostrictive actuator with AMA 400 or AMA 50 amplification developed by Cedrat Technologies contains a housing that prestresses the magnetostrictive rod and amplifies the displacement. This solution is patented by Cedrat Technologies and was initially used to manufacture amplified piezoelectric actuators.

Principle of operation

The operation of a magnetostrictive actuator (fig. 1.4) is as follows: the magnetostrictive core (4) is pre-tightened by means of the pretensioning spring (2). The magnetic bias field is produced by permanent magnets (1) and / or the bias coil, the current through the drive coil (3) generating the excitation magnetic field necessary for the controlled elongation of the magnetostrictive core. The elongation of the core is transmitted to the actuator of the actuator through the rod (5).

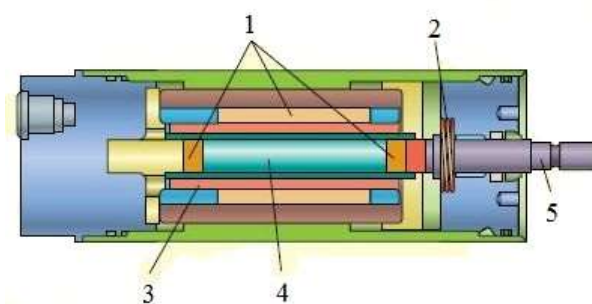


Figure 1.4 Simplified structure of a magnetostrictive actuator

permanent magnets (1), prestressing spring (2), drive coil (3), magnetostrictive core (4), drive rod (5),

For the analysis of magnetostrictive actuators we start from simplified structures such as the one shown in fig. 1.4, in which there are no temperature transducers, force sensors and other constructive elements. Only the basic phenomenon is analyzed to allow a predimensional and numerical simulation to optimize the structure, and additional elements will be introduced as sensitive points are identified.

1.4 Magnetostrictive actuator with planar coils

A new variant of magnetostrictive microactuator is the one that uses planar coils, coils that can be produced in large series at low costs. In fig. 1.5 is a schematic drawing of a planar coil magnetostrictive microactuators [9]. The component elements are: the actuating coils (1), the pre-magnetizing coils (2), the magnetostrictive core (3), the pre-magnetizing magnets (4), the elastic pretensioning element (5), the housing and the cover (6), and the actuating ring (7).

The pre-magnetization is provided by the pre-magnetization coils (bias), by the permanent magnets or by the combination of the two elements. This solution allows you to easily change the intensity of the magnetic field generated by the bias.

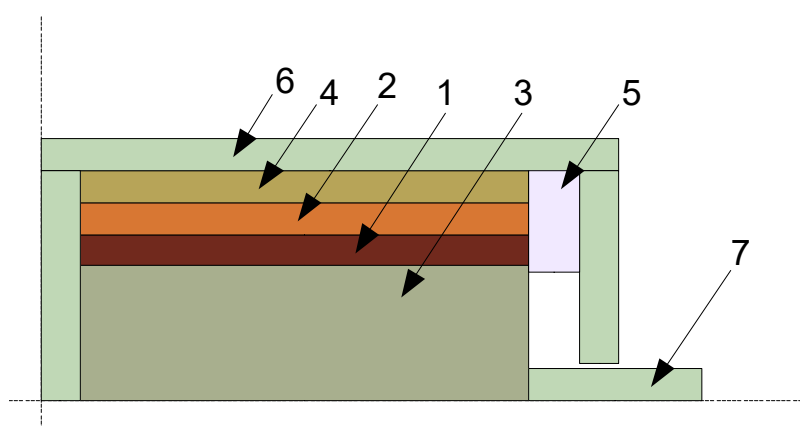
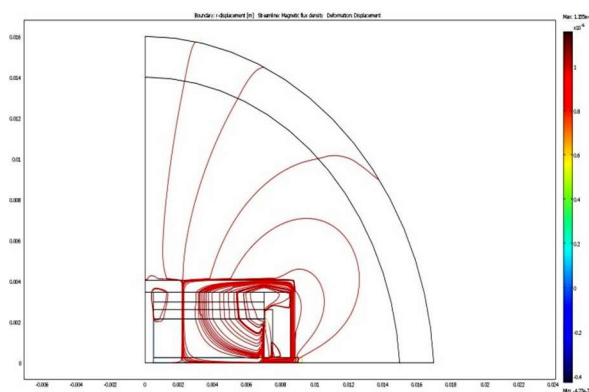


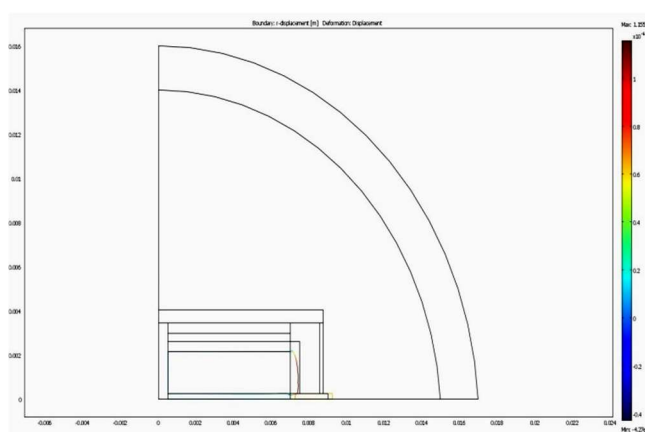
Figure 1.5 Schematic diagram of the magnetostrictive microactuator with planar coils

Actuating coil (1), pre - magnetizing coil (2), magnetostrictive core (3), pre - magnetizing magnet (4), elastic pretensioner (5), housing and cover (6), actuating ring (7).

Numerical results:



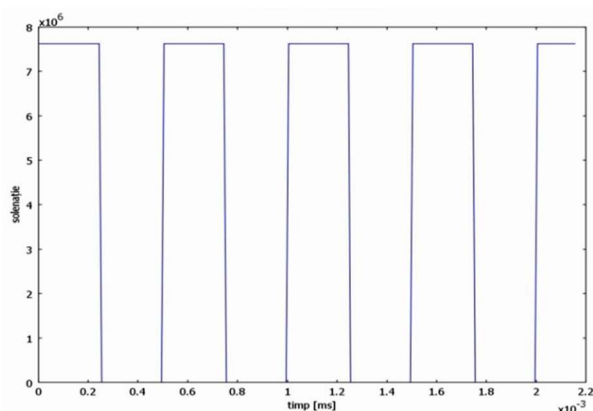
a) Magnetic flux density



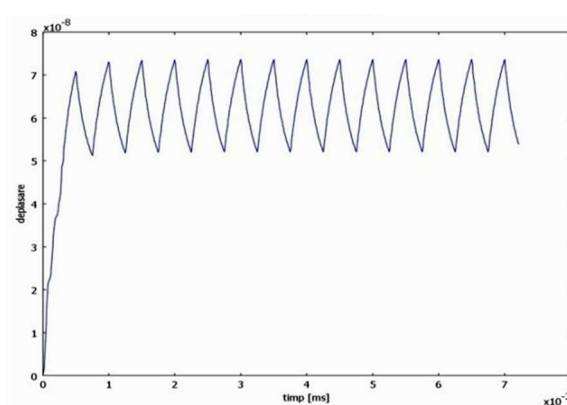
b) Drive ring displacement (max. 0.0868 μm , magnified 2592 times).

Figure 1.6 Numerical simulation results for the model microactuator with planar coils. Changes of the order of nanometers were obtained at maximum displacement, these coils can be used to calibrate the microactuator.

Because the drive and pre-magnetization coils (bias) are supplied with a 2kHz PWM signal with the same filling factor - adjustable by a parameter, we can assimilate the bias coils to drive coils. In dynamic mode, feeding the coils with a rectangular signal (fig. 1.7a) we obtain for the drive ring a displacement of approximately 20nm with the supply frequency of the coils.



a) Control signal (PWM).



b) The movement of the drive ring.

Figure 1.7 Dynamic planar coil microactuator operation.

1.5. Magnetostrictive actuator with cylindrical coils

The requirements for a linear magnetostrictive actuator for use in space require compliance with specific conditions related to operation in outer space: low energy consumption, power supply from solar panels (operating voltages in the range $18V_{DC}...32V_{DC}$), increased reliability / impossibility perform maintenance or repairs, operation in the absence of gravitational acceleration, radiation, working in a wide range of temperatures (day / night operation) and with a high temperature gradient (sunny face and shaded face).

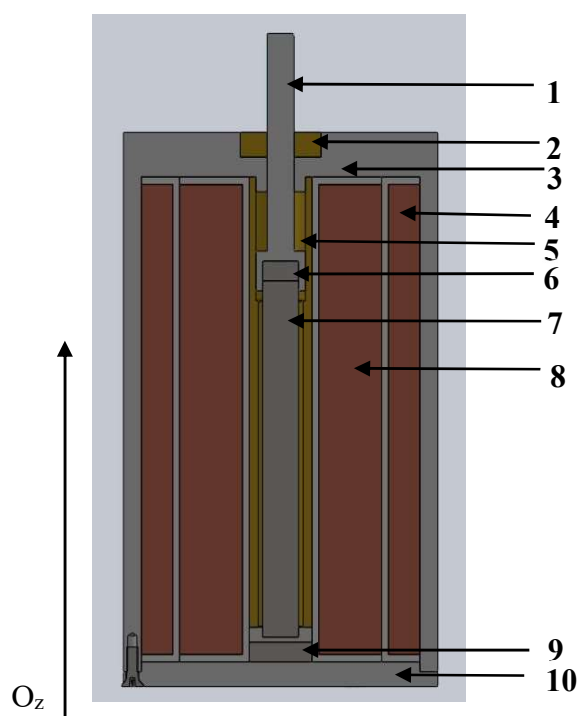
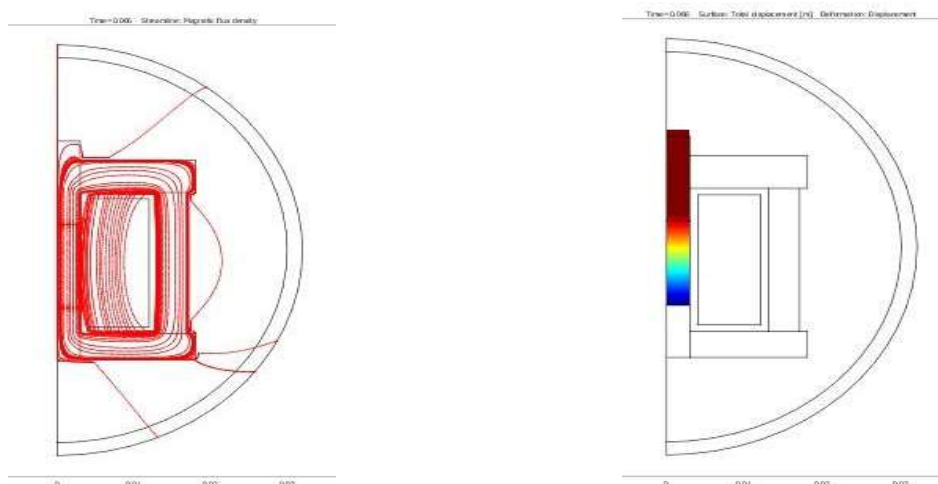


Figure 1.8 Magnetostrictive linear actuator, construction diagram

The construction diagram of the magnetostrictive actuator is shown in fig. 1.8: 1- shaft (drive rod), 2 - guide bush, 3- housing, 4 - magnetic bias coil, 5 - spring (mechanical bias), 6 - upper permanent magnet, 7 - Terfenol-D rod, 8 - coil drive, 9 - lower permanent magnet, 10 - cover. The operation of such a linear magnetostrictive actuator is based on the dimensional change of the rod (7) of magnetostrictive material (Terfenol-D) - under the cumulative action of the magnetic field and a spring (5).

Dimensioning / Simulation.

We opted for a classic structure with a cylindrical coil. The influence of the coil drive frequency with a PWM signal on the displacement was analyzed.



a) Magnetic flux density.

b) Displacement of the drive rod (magnified 300 times).

Figure 1.9 Results of numerical simulations for the classic microactuator model

As you increase the maximum signal frequency PWM trip rod decreases magnetostrictive actuator failing to meet excitation.

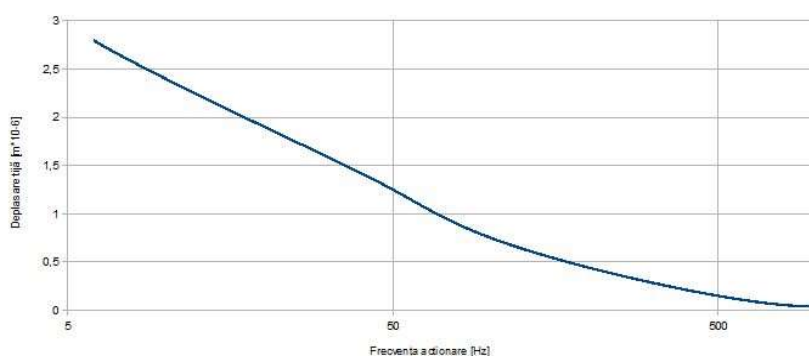
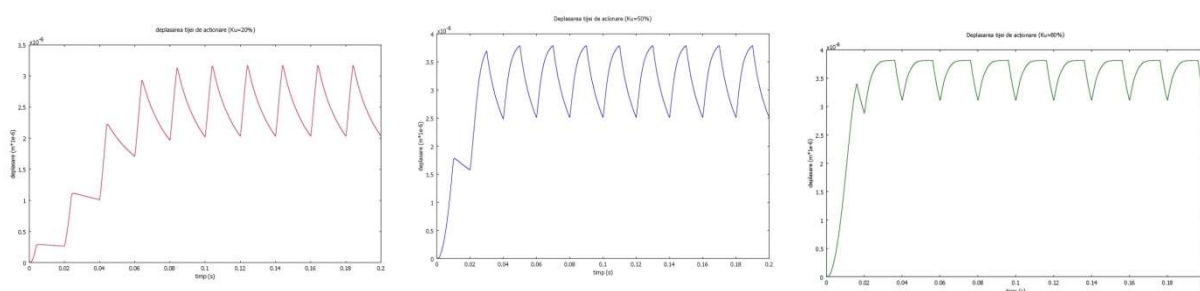


Figure 1.10 Displacement of the rod depending on the operating frequency (log)

The results obtained by varying the filling factor of the PWM signal show a different transient regime, from $80\mu s$ for $K_U = 20\%$ to $20\mu s$ for $K_U = 80\%$.



a) $K_U = 20\%$

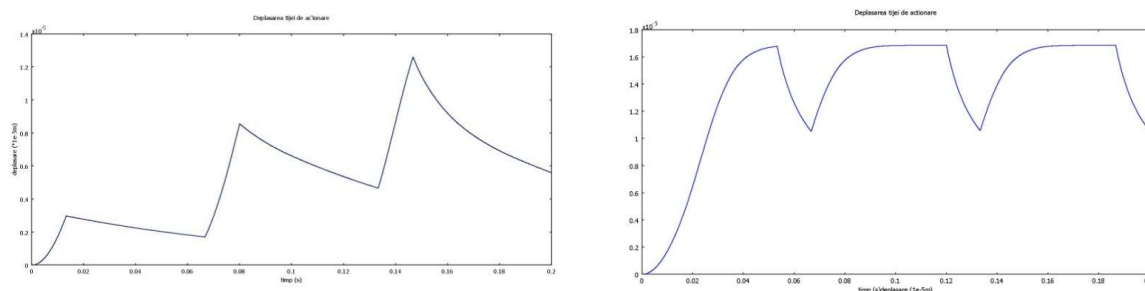
b) $K_U = 50\%$

c) $K_U = 80\%$

Figure 1.11 Displacement of the drive rod at PWM controls with variable K_U filling factor ($f = 50\text{Hz}$)

In order to analyze the operation of microactuators in the case where there are two coil - coil magnetization (bias) and a control / drive - from the previous model, split coil current in two parts with equal sections, each coil while maintaining the same current tip through turns.

Using a filling factor $K_{bias} = 80\%$ for the premagnetization signal (bias) and a filling factor $K_{act} = 20\%$ for the actuation signal, the results presented in fig. 1.12. Placing the drive coil inside maximizes travel.



a) drive coil inside

b) coil of bias inside

Figure 1.12 Numerical simulation results for the two-coil model. Filling factor $K_{act} = 20\%$ for drive and $K_{bias} = 80\%$ for bias ($f = 15\text{Hz}$)

In order for the actuator to be used for a wide range of applications, a variable filling factor in the range of 10% - 90% and a working frequency in the range of 20Hz - 12kHz is required. To test the actuator response beyond these limits it is necessary for the control system to be able to provide higher operating frequencies, up to 20kHz. The time diagram of the signals is that of fig. 1.13.

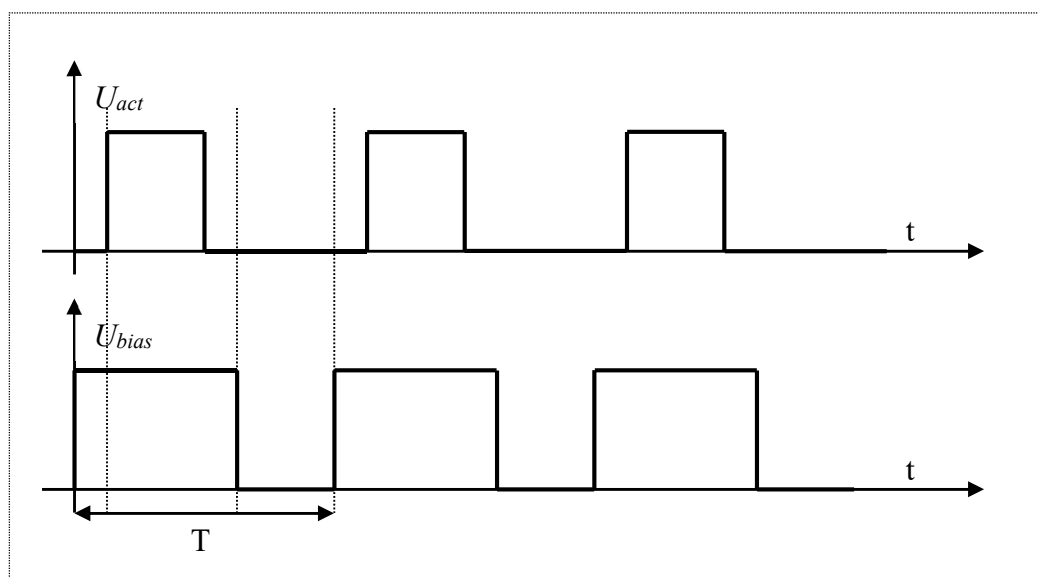


Figure 1.13 Waveforms for voltages applied to the drive coil and on the magnetic bias coil
 U_{act} – voltage at the terminals of the drive coil,

U_{bias} – voltage at the terminals of the magnetic bias coil,

$K_{act} = 10\% \div 90\%$, typical 40% - the filling factor for the voltage U_{act} ,

$K_{bias} = 15\% \div 95\%$, typical 50% - the filling factor for the voltage U_{bias} ,

$f_{act} = f_{bias} = 20\text{Hz} \div 20\text{kHz}$.

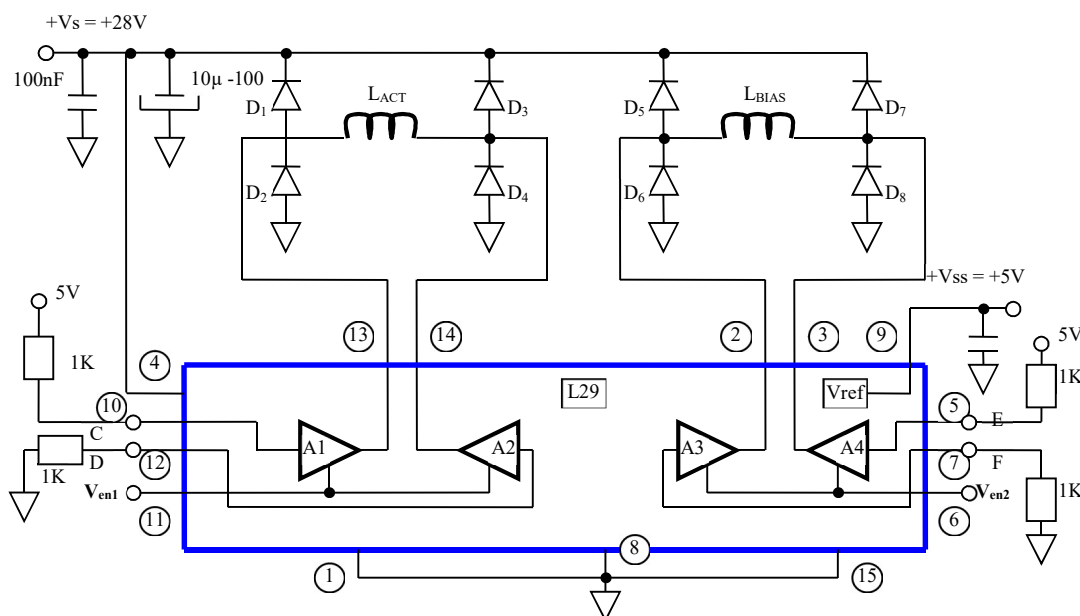


Figure 1.14 Diagram for the bridge control of the drive and activation coils (magnetic bias). To control the coils, a control board was designed and made that allows the supply of coils modulated in frequency. The bridge has two logic activation inputs (V_{en1} and V_{en2}) and a maximum current (peak value) of 4A.

1.6. Practical realization of linear magnetostrictive actuators

In order to validate the solutions obtained from the numerical simulations, we practically made a small magnetostrictive actuator with which we performed tests.

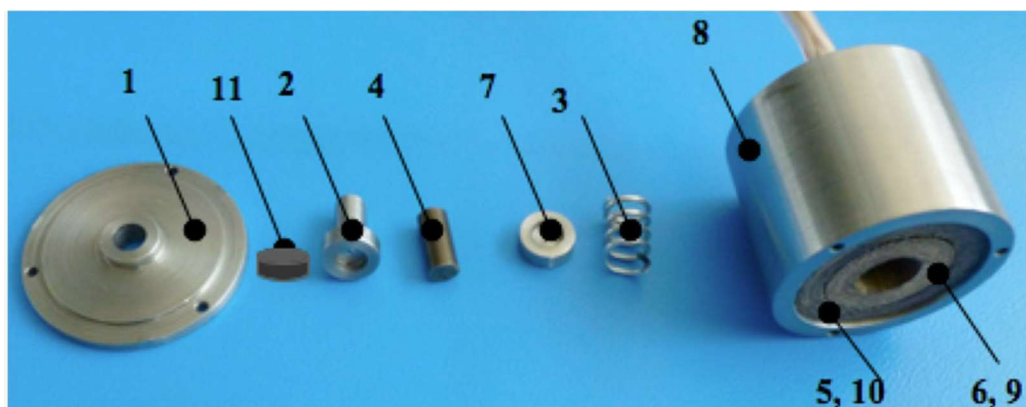


Figure 1.15 Linear magnetostrictive actuator: 1 cover, 2 rod, 3 spring for prestressing, 4 cylinder of Terfenol-D, 5 bias coil, 6 activation coil, 7 lower positioning element, 8 housings, 9 spool (support) for activation coil, 10 spool (support) for polarization coil, 11 permanent magnet for polarization. Physically made components.

The magnetostrictive linear motor is driven by the electronic command and control blocks.

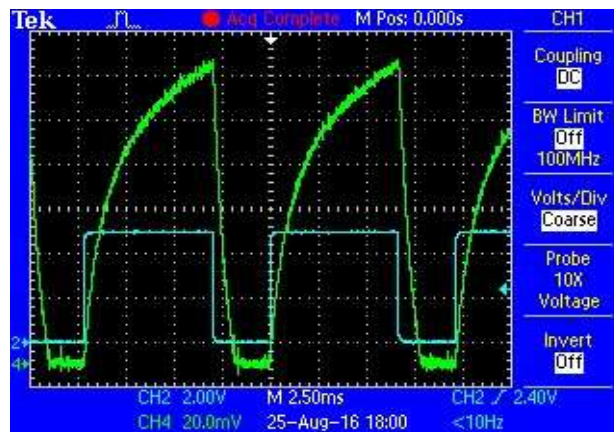
The magnetic bias coil ensures - together with the permanent magnets - the static operating point of the linear motor. The actuator coil provides the magnetic field required for the active material of the actuator to move in a controlled manner.

1.7. Structural optimization (constructal) of the model, realization and testing of the improved variant. Experimental tests..

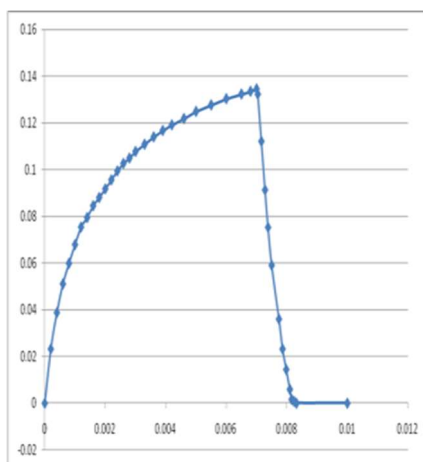
The magnetostrictive material (Terfenol – D) is in finite amount. A first optimization step for this actuator variant refers to the amount of permanent magnet for which, at a given excitation, the linear displacement of the actuator shaft is maximum. A second stage of optimization refers to the optimal distribution of the magnetic material (permanent magnet) and the magnetostrictive material in the central column of the magnetic circuit of the actuator.

To optimize the amount of magnetic material and its optimal distribution in the central column of the magnetostrictive actuator, a simplified design was used, which retains only the components strictly necessary in its operation and sizing. The mathematical model used is the simplified model, 2D axial – symmetrical, which uses the axial symmetry of the device and allows the reduction of the numerical solving effort, including the necessary calculation time.

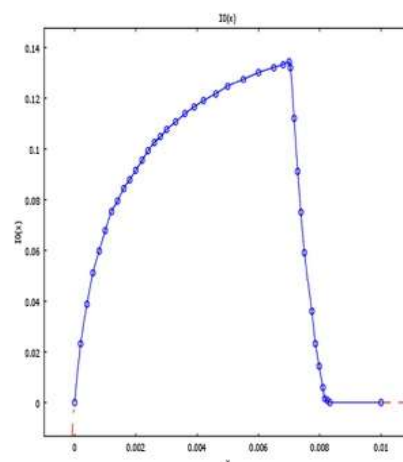
The disadvantage of this approach is that the electrical excitation must be introduced by current and not by voltage - the physical actuator being controlled by modulated voltage pulses (PWM). This difficulty is (partially) removed by the introduction of currents with waveforms similar to those recorded during the tests of the physically performed actuator.



a) Actuation voltage and current.



b) Actuation current, digitized signal.



c) Actuation current used in the simulation.

Figure 1.16 Actuation current, $f = 100$ Hz, $k_{act} = 70\%$.

To obtain a simulation close to the experimental conditions, current waveforms purchased from a physically performed and tested actuator were used.

The simulations used a total volume of active magnetic material of approx. 600 mm^3 ($189\pi \text{ mm}^3$) - permanent magnet and magnetostrictive material (Terfenol – D).

Deoarece curentul de activare (bias) trebuie să premagnetizeze (să activeze magnetic), materialului magnetostrictiv, factorul de umplere al acestui curent, k_{bias} , trebuie să acopere (temporal) factorul de umplere al curentului de acționare, k_{act} . Prezintă rezultatele obținute pentru valori fixate ale factorilor de umplere: $k_{act} = 70\%$ (acționare) și $k_{bias} = 80\%$ (bias). Folosind curenți PWM crenel s-a obținut deplasarea tijei de acționare cu un maxim cvasistaționar de $4,850\mu\text{m}$, ca în fig. 1.17.

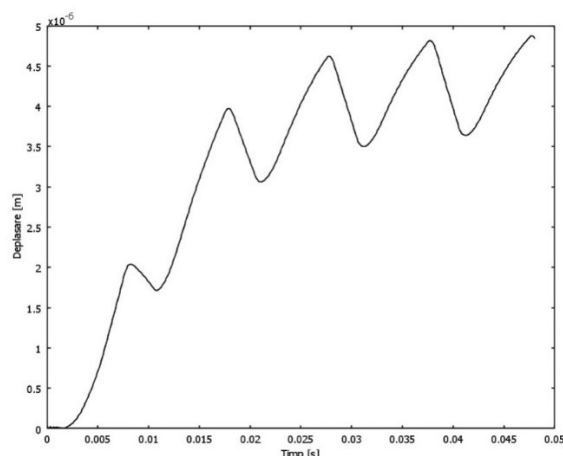


Figure 1.17 Moving the drive rod, $f = 100 \text{ Hz}$, $k_{act} = 70\%$, step current (crenel).

To evaluate a behavior close to the actual situation of the actuator, waveforms were used in which the “on” interval of the bias current starts in advance and ends late, by 0.5 ms, compared to the “on” interval of the bias current. drive current.

With these input data, the displacement of the actuating rod with a maximum of $4,353 \mu\text{m}$ was obtained (fig. 1.18). It should be noted that the analysis of the actuator behavior at the step current (ideally) is purely theoretical, leading to overestimated results for the displacement of the drive rod.

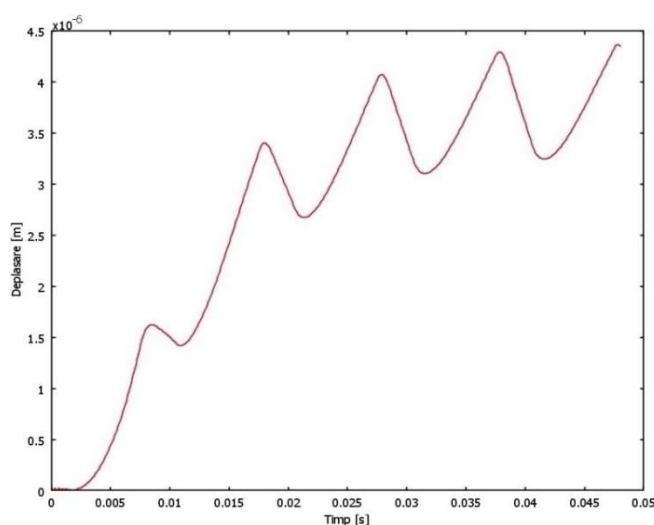


Figure 1.18. Moving the drive rod, $f = 100 \text{ Hz}$, $k_{act} = 70\%$, real current (measured).

For a first iteration regarding the optimization of the volumetric ratio between the permanent magnet and the magnetostrictive material in the active column, we generated geometries in which the permanent magnet volume was axially segmented and the resulting segments were interspersed in the correspondingly divided Terfenol – D column. The height of the permanent magnet segments was between 1 mm and 10 mm (volumes being between $9\pi \text{ mm}^3$ and $90\pi \text{ mm}^3$).

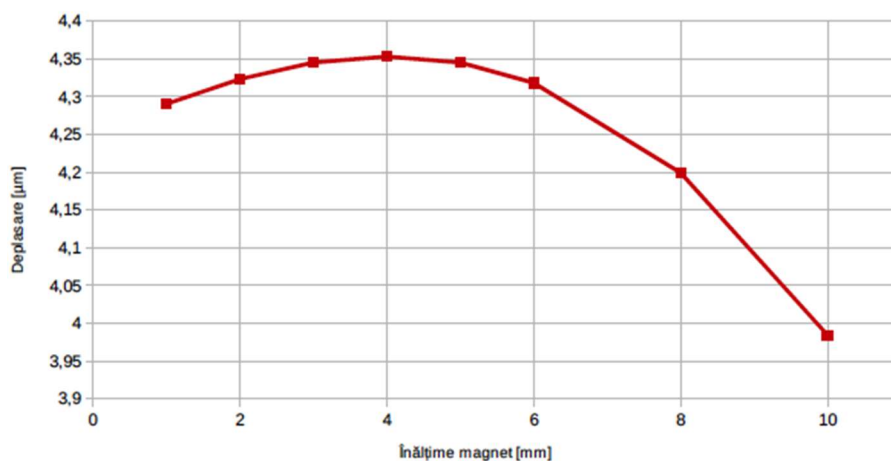


Figure 1.19 Displacement of the actuating rod depending on the height of the permanent magnet.

Optimizing the volumetric ratio between the permanent magnet and the magnetostrictive material in the active column by varying the height of the permanent magnet between 1 mm and 10 mm (volumes between $9\pi \text{ mm}^3$ and $90\pi \text{ mm}^3$) led to maximum displacements of the actuating rod between $3,984 \mu\text{m}$ and $4,353 \mu\text{m}$. The maximum that appears for the height of 4 mm of the permanent magnet is observed.

To optimize the distribution of the magnet volume and the magnetostrictive material in the active column, we generated geometries in which the permanent magnet volume of $36\pi \text{ mm}^3$ was cut into two, three and four equal volumes. Also, the volume of Terfenol-D of $153\pi \text{ mm}^3$ was cut into three, four and five equal volumes, respectively, being interspersed with the volumes of permanent magnet.

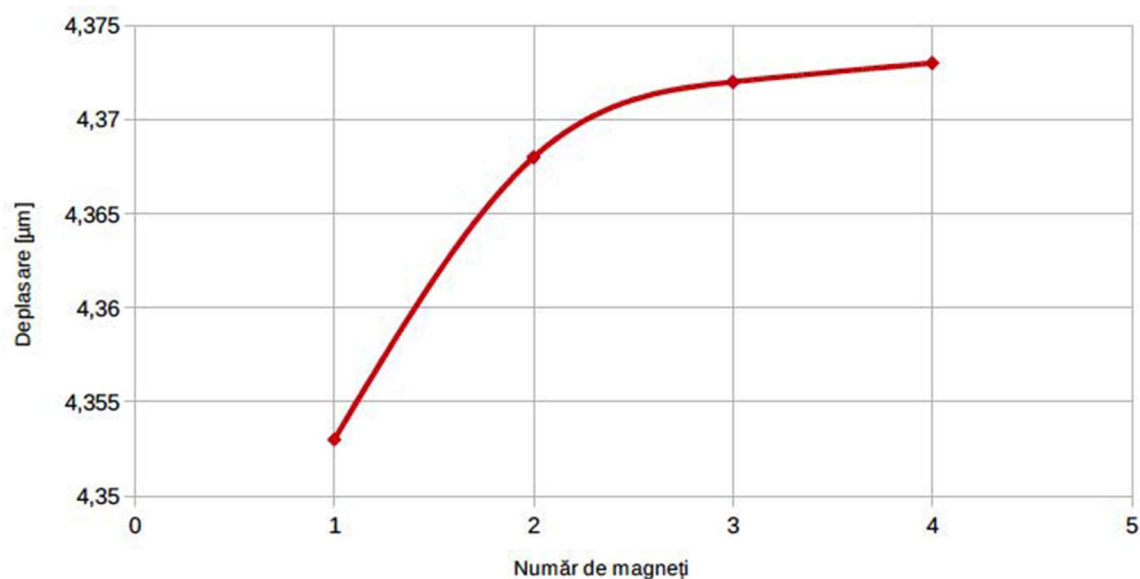


Figure 1.20 Displacement of the drive rod according to the number of magnets (constant total volume).

For the entire permanent magnet volume and then divided into two, three and four volumes (segments), maximum displacements of the drive rod of 4,353 μm , 4,368 μm , 4,372 μm and 4,373 μm , respectively, were chosen.

It is noted that the maximum has not yet been reached, but technological difficulties do not justify the cutting of permanent magnets with a height of less than 1 mm.

The analysis of the magnetostrictive actuator was extended to a 3D model, an approach that allowed the simulation of the voltage supply and not PWM current.

The current of the two windings (actuation and premagnetization) at the PWM supply in voltage are represented in fig. 1.21.

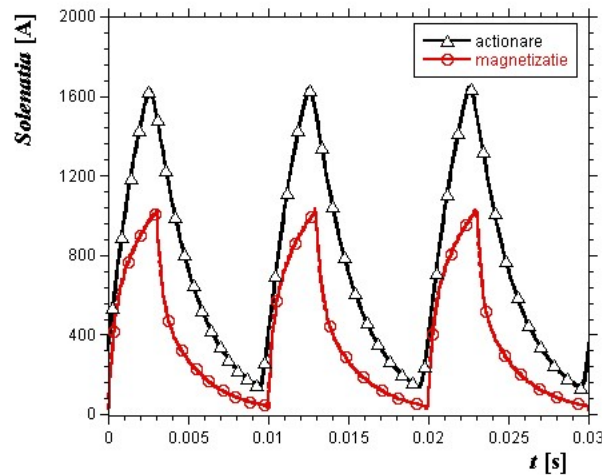
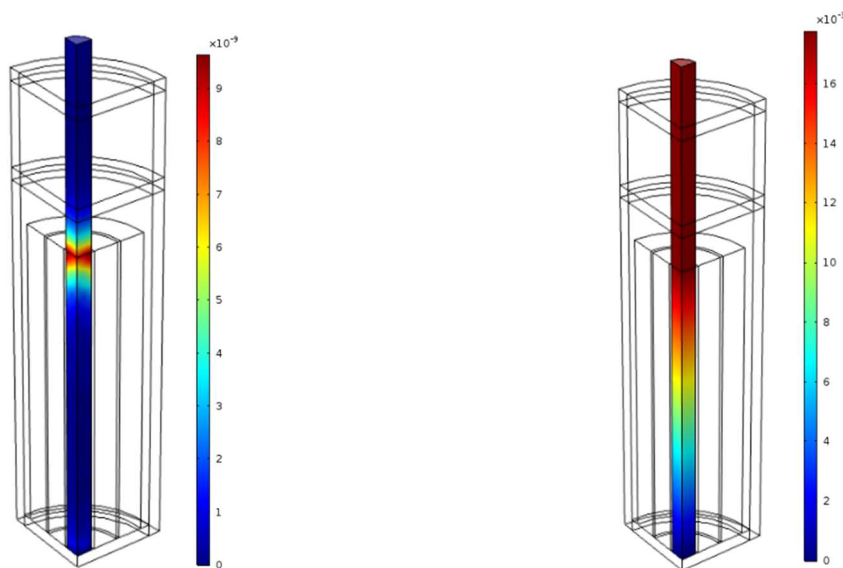


Figure 1.21. Actuation and pre-magnetization currents for PWM supply, in voltage ($5\text{V}, f = 100 \text{ Hz}, k = 30\%$).

The simulations started from the initial state of rest (zero initial conditions), the movement of the movable rod at two moments of time being shown in fig. 1.22, highlighting the deformation before and after reaching the quasi-stationary regime.



a. At the beginning of the deformation. b. After reaching a quasi-stationary regime.

Figure 1.22. Movement of the actuator rod (mm) in the direction Oz at two time points.

The supply of the actuating and pre-magnetizing coils of the step actuator voltage causes a non-linear variation of the inductive current, in accordance with the actual operation.

A possibility of optimizing the actuator is the geometric optimization, in terms of form factor (also called aspect ratio, representing the ratio height / radius = L / R). Starting from an initial value of the L / R ratio, as a reference (Fig. 1.23) and keeping constantly the volume of magnetostrictive material that the designer decides to use, the displacement for different L / R values is determined. Figure 1.23 shows the deformations for two variants: the reference model and the model with the optimized form factor, with the deformations (marked in red) amplified for a better visualization.

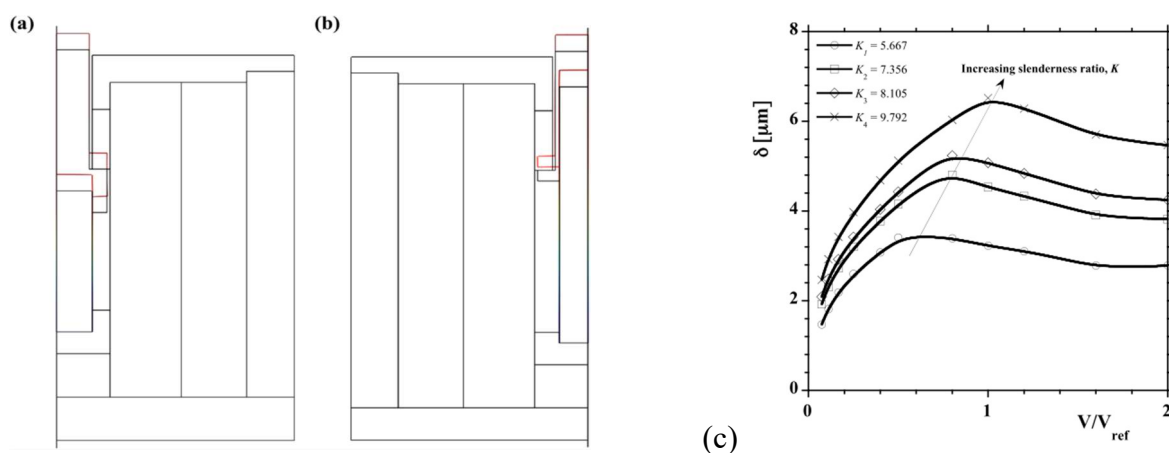


Figure 1.23. Magnetostrictive actuators - reference model and model with optimized form factor (a) for $L/R = 4$, the maximum displacement is $2.8\mu\text{m}$. (b) for the actuator with the optimized form factor ($L/R = 8.1$), the maximum displacement is $4.7\mu\text{m}$. (c) optimizing the displacement according to the geometric form factor and the volume of magnetostrictive material

The increase of the height and the decrease of the radius of the rod of magnetostrictive material determines the increase of the maximum displacement, until the appearance of the magnetic saturation.

In order to test the functional model of magnetostrictive actuator, it was necessary to make the electronic command and control stages. Thus, printed circuits were made for the electronic coil command and control module, for the power module, for the control module of the Peltier elements as well as the necessary modules for power supply and voltage stabilization. As an example, the electronic power module for driving the coils of the linear magnetostrictive actuator is shown in Figure 1.24.

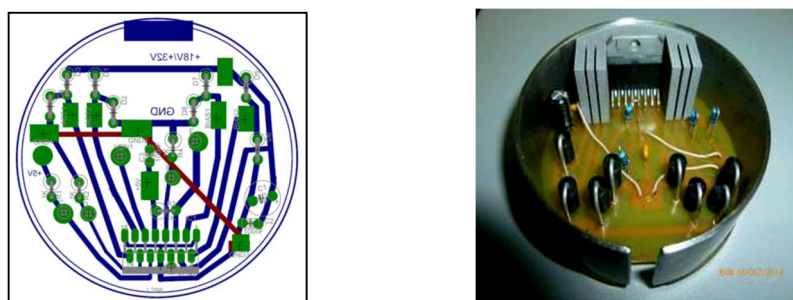


Figure 1.24. Printed circuit of the electronic power module for driving the coils, CAD project and practical realization equipped with electronic components.

Testing the functional model of the magnetostrictive linear actuator

To determine the forces developed by the magnetostrictive linear actuator, it was tested in the Test Laboratory within SC STRAERO SA. The test method consisted in generating and measuring the force developed by the linear magnetostrictive actuator.

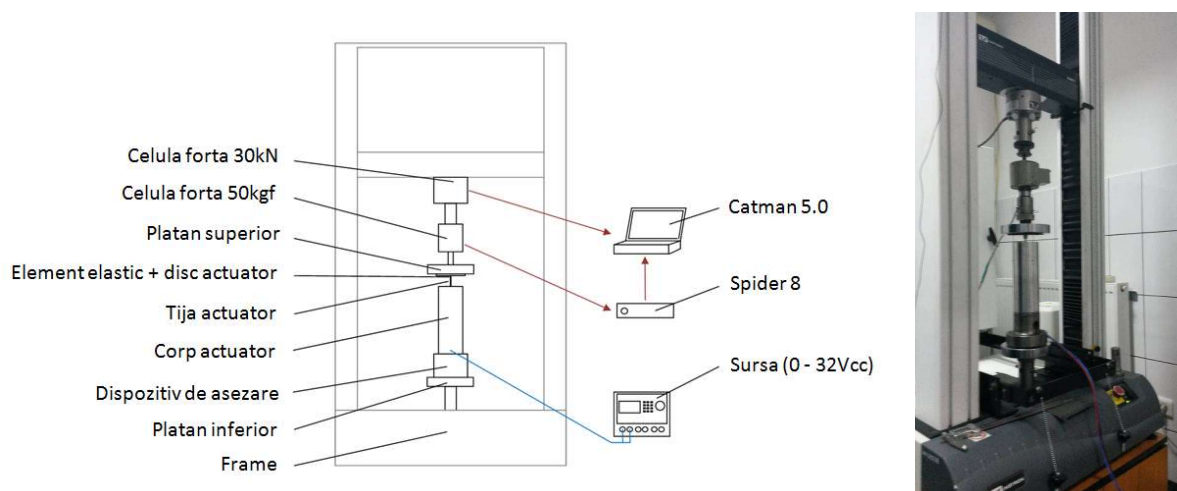


Figure 1.25. Test equipment with actuator mounted - components and configuration used in practice.

The following is an example with the signal representing the force developed by the linear magnetostrictive actuator, for the supply voltage of 18 V_{DC}.

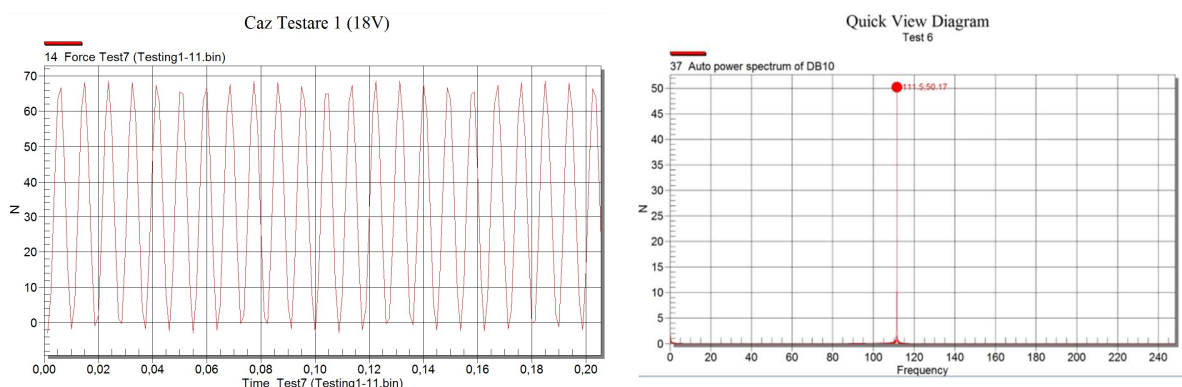


Figure 1.26. The force developed by the magnetostrictive linear actuator as a function of the supply voltage at the operating frequency of 111.5 Hz

To measure the peak-to-peak amplitude of the mechanical oscillation performed by the mobile equipment of the magnetostrictive linear actuator, a measuring system using Agilent 5529B interferometer was used.

The variation of the amplitude of the mechanical oscillation made by the magnetostrictive core as a function of time for $f = 100$ Hz is presented (figure 1.27), the peak-to-peak amplitude of the mechanical oscillation is $A_{100} = 30 \mu\text{m}$.

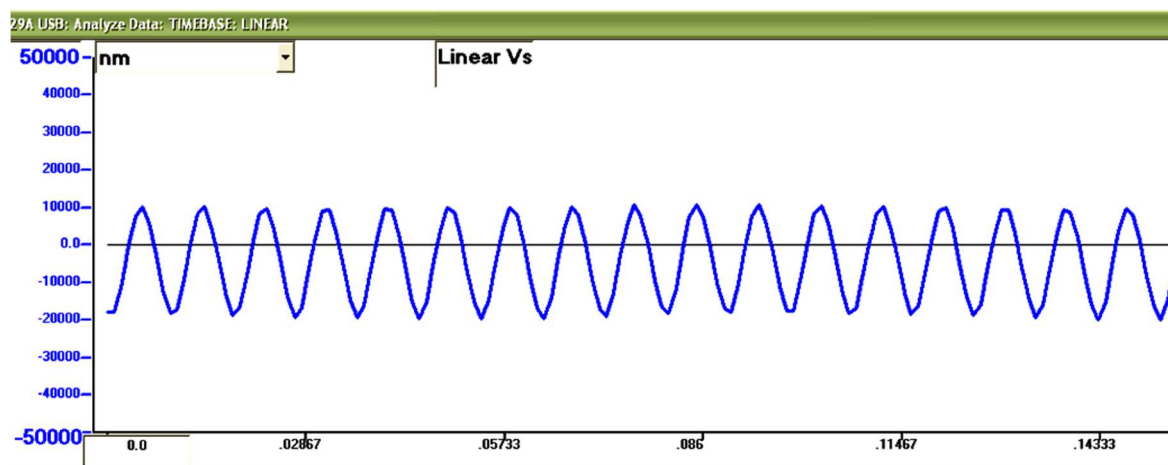


Figure 1.27. Displacement of the magnetostrictive core as a function of time, for PWM voltages with $f = 100$ Hz, $U = 32$ V_{PP}, the filling factor for the activation coil $k = 70\%$ and $k = 40\%$, for the magnetic bias coil.

To determine the current absorbed at the terminals by the magnetostrictive linear actuator, for different operating regimes, measurements were performed for an operation in the frequency range $f = 10\text{Hz} \div 21\text{kHz}$, powered at 18 V_{PP} and having a filling factor of $k = 50\%$, $k = 70\%$ and $k = 80\%$ applied to the activation coil voltage and a DC supply voltage of 28 V_{dc} applied to the magnetic bias coil. The following is an example.

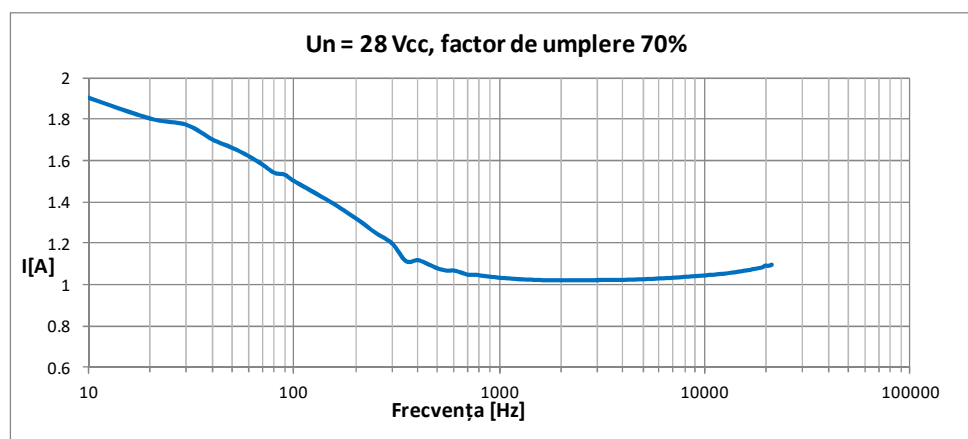
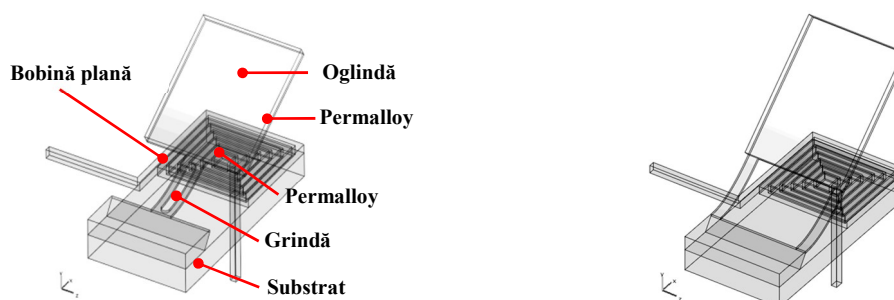


Figure 1.28. Current absorbed by the magnetostrictive linear actuator. $f = 10\text{Hz} \div 21\text{kHz}$, $U = 18$ V_{PP}, $k = 70\%$, for the activation coil. $U_2 = 28$ V_{dc}, $k = 100\%$ for magnetic bias coil.

CHAPTER 2

ELECTROMECHANICAL ACTUATORS

Cantilever electromagnetic actuators (with beam) are devices made up of structural parts, magnetic materials and interacting electrical coils. The extruded actuator is provided with a magnet at the free end of a polyamide console (beam). The magnet interacts with a flat spiral coil located on a rigid substrate with a supporting role (Fig. 2.1). The upper surface of the movable element is mirror type and allows the controlled deviation of an incident light beam, deviation proportional to the angle of inclination of the mirror. The control for adjusting the angle of inclination is provided by the value of the electric current injected into the coil. In this variant there is no position sensor for the mobile element and feedback loop.



a. Cantilever electromagnetic actuator with a central beam. *b.* Cantilever electromagnetic actuator with two side beams.

Figure 2.1 Console type electromagnetic actuators - CAD sketch. Approximate dimensions for the non-powered actuator (at rest): 2.5 mm × 1.25 mm × 0.45 mm.

Because numerical simulation is performed on three-dimensional computational domains, it is useful to simplify the models to reduce the computational time. Thus we replaced the flat coil with rectangular, concentric turns (Fig. 2.2). The symmetry given by the xOy median plane was used to halve the computational domains. The validity of the results can be verified later by comparison with the complete models.

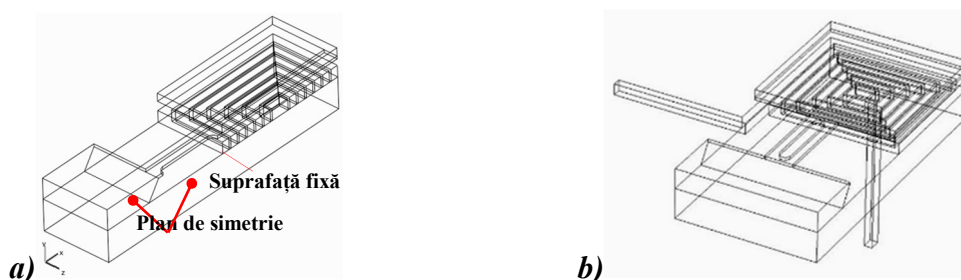
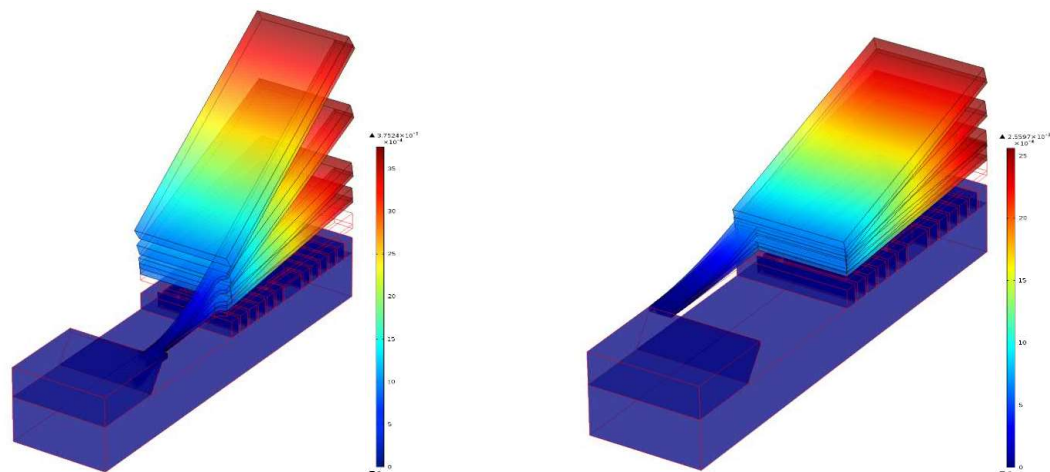


Figure 2.2 Calculation domains for the console type electromagnetic actuator with a central beam: a) using symmetry, with the coil consisting of concentric turns; b) without using symmetry, with spiral coil.

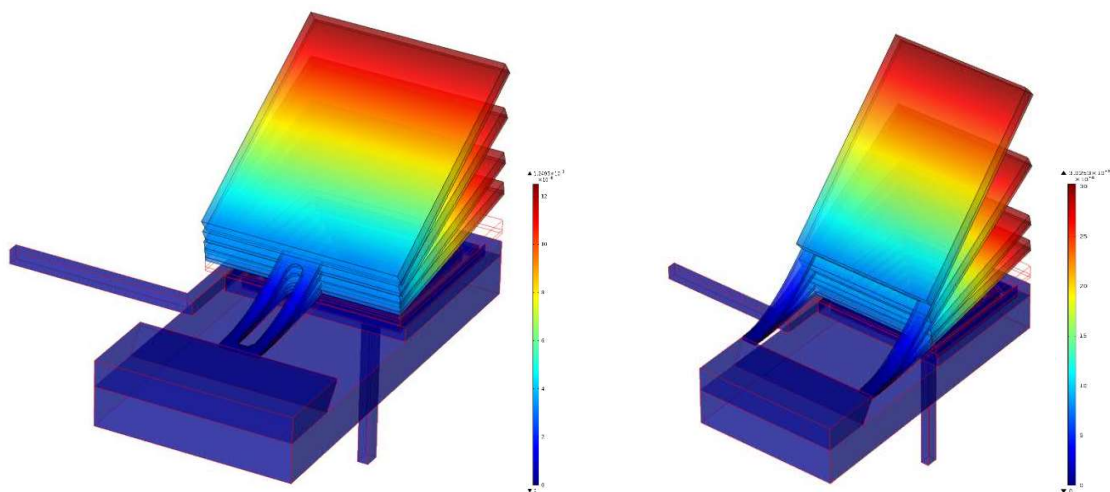
The deviation of the mirror and the first six eigenmodes of structural deformation are evaluated qualitatively for two actuator variants, obtained by using simplified and complete models (Fig. 2.2).

Regarding the performance, fig. 2.3 shows, through color maps, the deformations for four operating points.



a) Cantilever type electromagnetic actuator with a central beam, $A = 2$, maximum deformation = 1.876 mm.

b) Cantilever type electromagnetic actuator with two side beams, $A = 2$, maximum deformation = 1,280 mm.



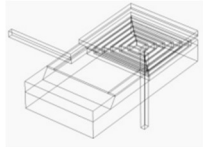
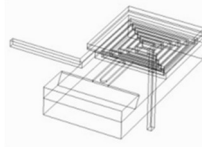
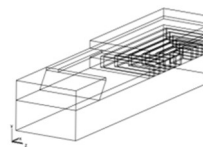
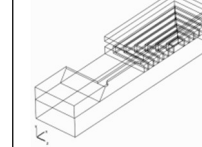
c) Cantilever type electromagnetic actuator with a central beam, maximum deformation = 1.295 mm.

d) Cantilever type electromagnetic actuator with two side beams, maximum deformation = 1.511 mm.

Figure 2.3 Deformations of the moving element in stationary conditions. The results for a) and b) are scaled by 2

Deviation angles (in degrees) are calculated using the maximum deformation in the vertical direction (Oy) and shown in Table I. The length of the beam at rest is 2 mm.

Table I Deflection angle.

	a)	b)	c)	d)
Relative permeability, μ_r .				
10	6,45°	7,02°	6,03°	7,98°

5	12,67°	13,87°	11,31°	15,92°
2	27,60°	29,03°	22,26°	35,42°
1	49,06°	55,81°	52,60°	69,55°

For complete models, the mirror is deposited on an additional polyamide sheet, with similar dimensions.

Regarding the structural (modal) analysis, using the simplified models (Fig. 2.2a) with $\mu_r = 1, 2, 5, 10$, $B_r = 0.37$ T, and $J_n = 6$ A / mm², in fig. 2.4 shows the qualitative deviation of the movable element and the mirror for the first six structural modes. Due to the limitations imposed, the deformations keep the symmetry of the models.

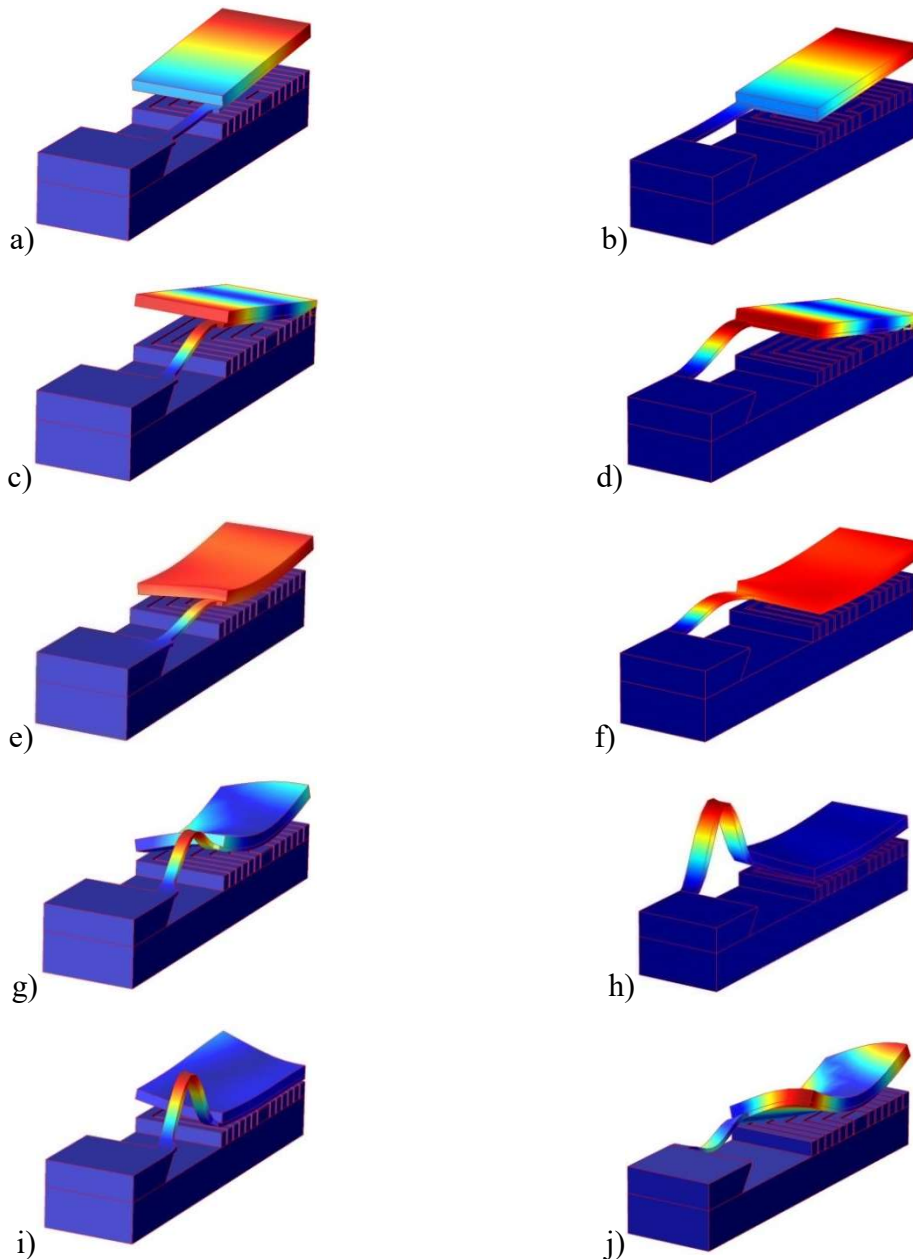
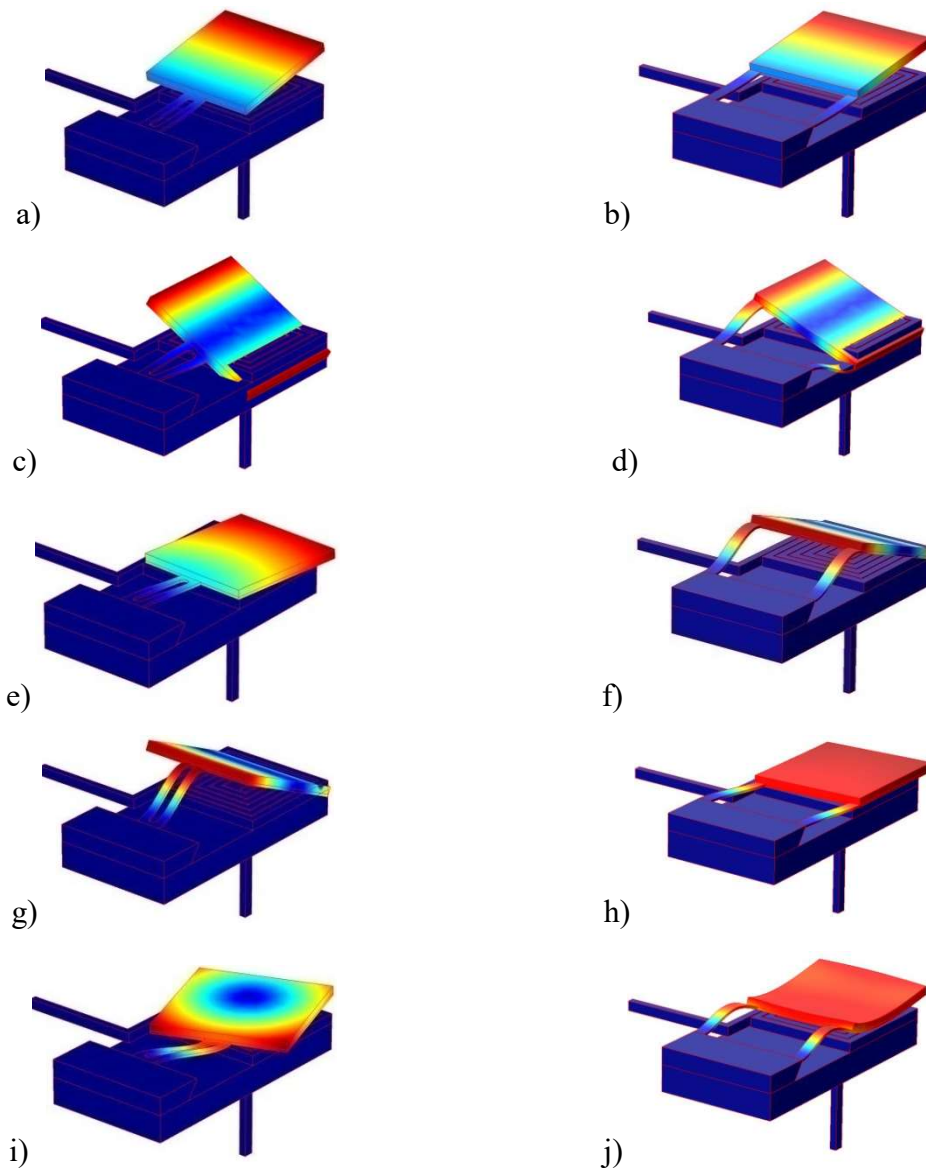




Figure 2.4 Deformations for the first six eigenstructural modes. The results for the left column (console with a central beam) are scaled by 2.5 and for the right column (console with two side beams) by 2.

Using the complete structure of the actuator and the spiral structure of the flat coil, the results appear as in Figure 2.5.



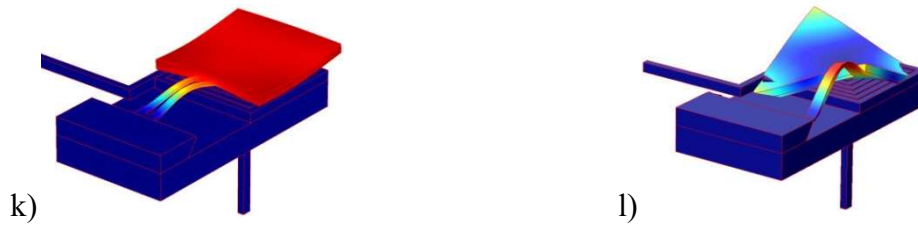


Figure 2.5 Deformations for the first six eigenstructural modes. The results for the left column (console with a central beam) are scaled by 6.25 and for the right column (console with two side beams) by 4.5.

Analyzing comparatively the results obtained for the reduced and full models (Fig. 2.4 vs Fig. 2.5) under the same working conditions, we observe that the deformations obtained on the complete model move away (except for the first mode) from the symmetry with respect to the xOy plane. Except for the first proper mode, the deformations move away from the symmetry around the xOy plane. This result involves the use of a complete representation of the actuator when analyzing the structural behavior.

CHAPTER 3

PIEZOELECTRIC ACTUATORS

Rotating piezoelectric motors are motors that obtain torque using the frictional force between a cylinder, ring or disc made of composite piezoelectric material and a metal ring that constitutes the rotor. The operation of these motors is done by means of a traveling wave, a wave obtained by the proper excitation of the rotor. To obtain high amplitudes of the traveling wave, the stator is excited in the resonant frequency zone. At the base of the operation is the inverse piezoelectric effect, an effect that produces the rotational motion by bending the stator due to a traveling wave, a wave obtained by superimposing two waves in the quadrature. The traveling wave produces an elliptical motion of the stator surface and transmits the motion by direct contact with the rotor.

For the study by numerical modeling of the operation of the rotating piezoelectric motor, the active piezoelectric cylinder (PZ) was modeled, a cylinder that constitutes the stator of the rotating piezoelectric motor.

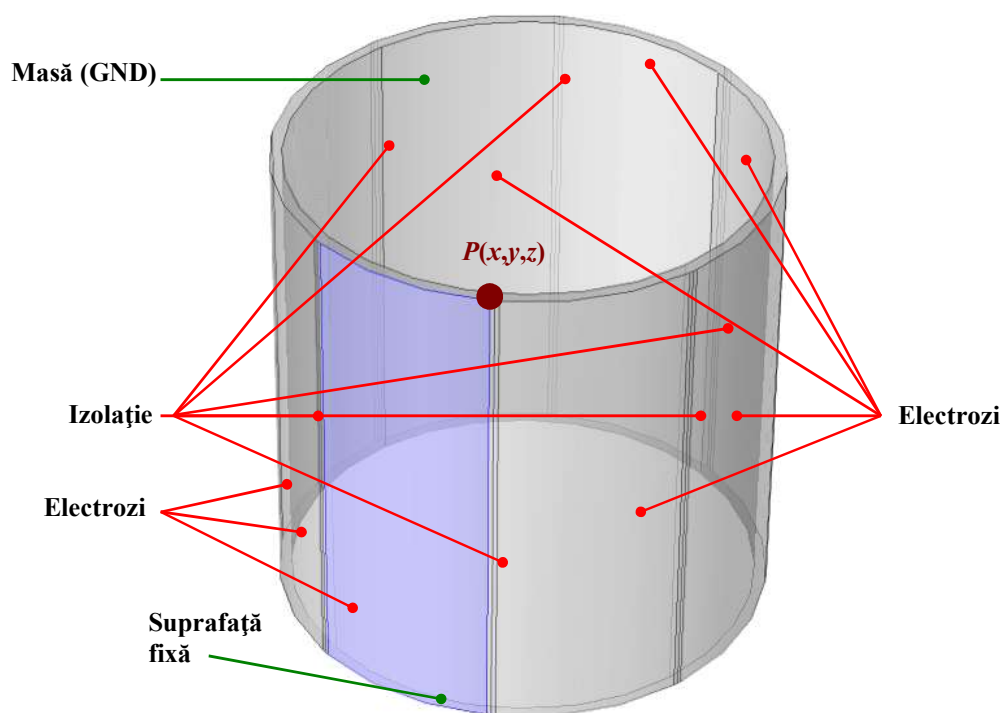


Figure 3.1 Field of calculating the PZT piezoelectric cylinder (PIC255) - positioning the electrodes.

The boundary conditions that close the problem are specified in Figs. 3.1, which presents the calculation range: imposed electric potentials, successively phased with $\pi / 4$ rad (electric angle) for the electrodes on the outer side surface of the part compared to the inner side surface of the part (which is at zero potential, ground), insulation (zero electric charge density) for the spaces between the electrodes and the upper and lower horizontal faces; the lower horizontal surface is fixed and the other surfaces are sliding. 3D analysis of the operation of the piezoelectric cylinder

is required. The transitional regime is conveniently delimited so that the quasi-stationary state is reached.

Numerical simulations were performed for the working frequency of 30 kHz and the peak value of the supply voltage of 50 V. Figure 3.2 shows the displacement of the material point $P(x, y, z)$ (figure 3.1), the driving torque (oriented in the vertical direction) and the driving force in the horizontal plane - calculated at the level of the drive surface of the rotor (xOy plane, upper surface).

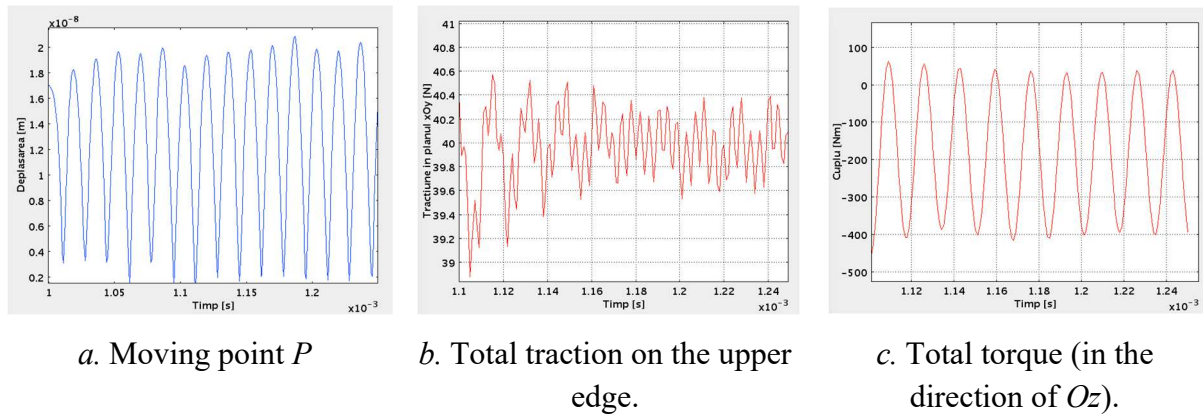
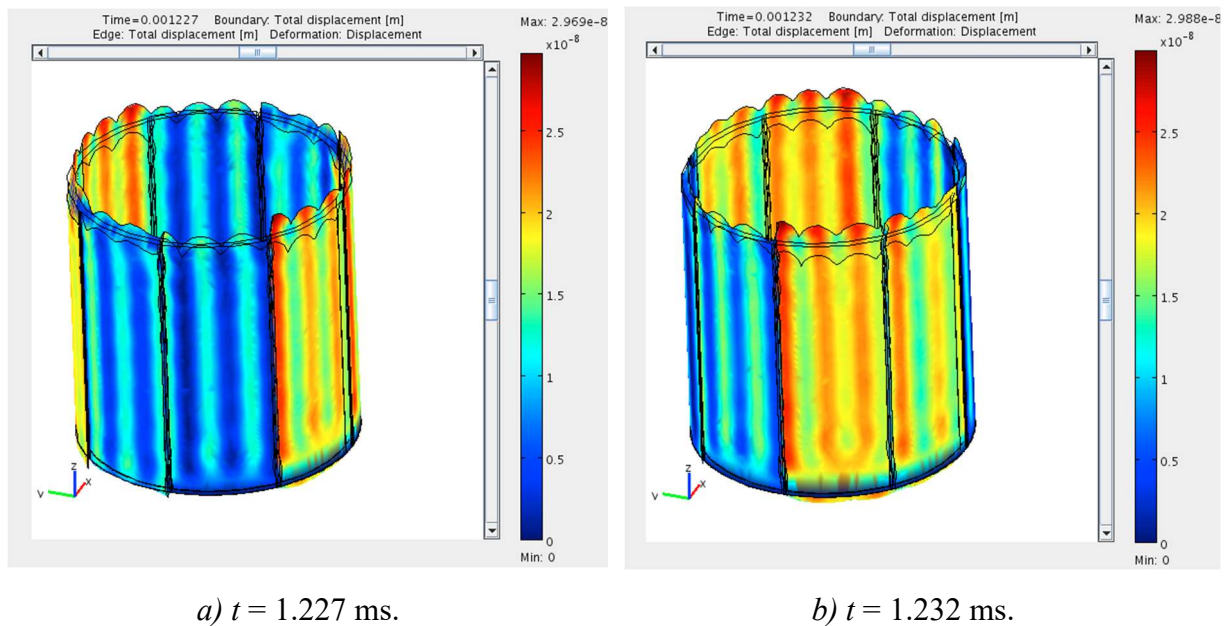
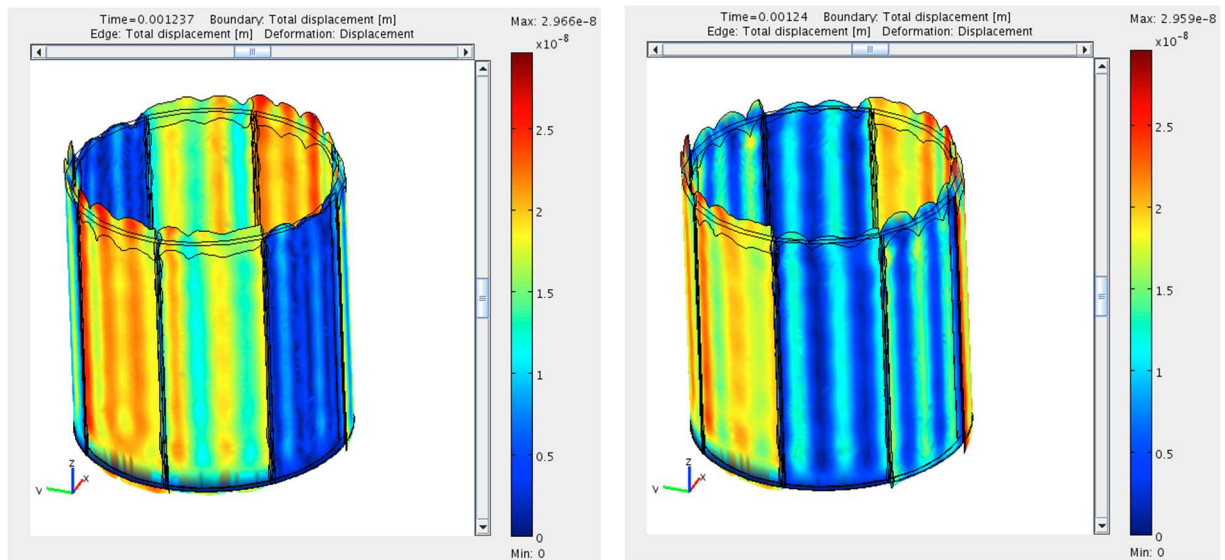


Figure 3.2. Piezoelectric rotor dynamics.

The deformation of the PZ tube under the action of the traveling wave is shown, in figure 3.3, at four moments of time representing a quasi-period of entrainment.



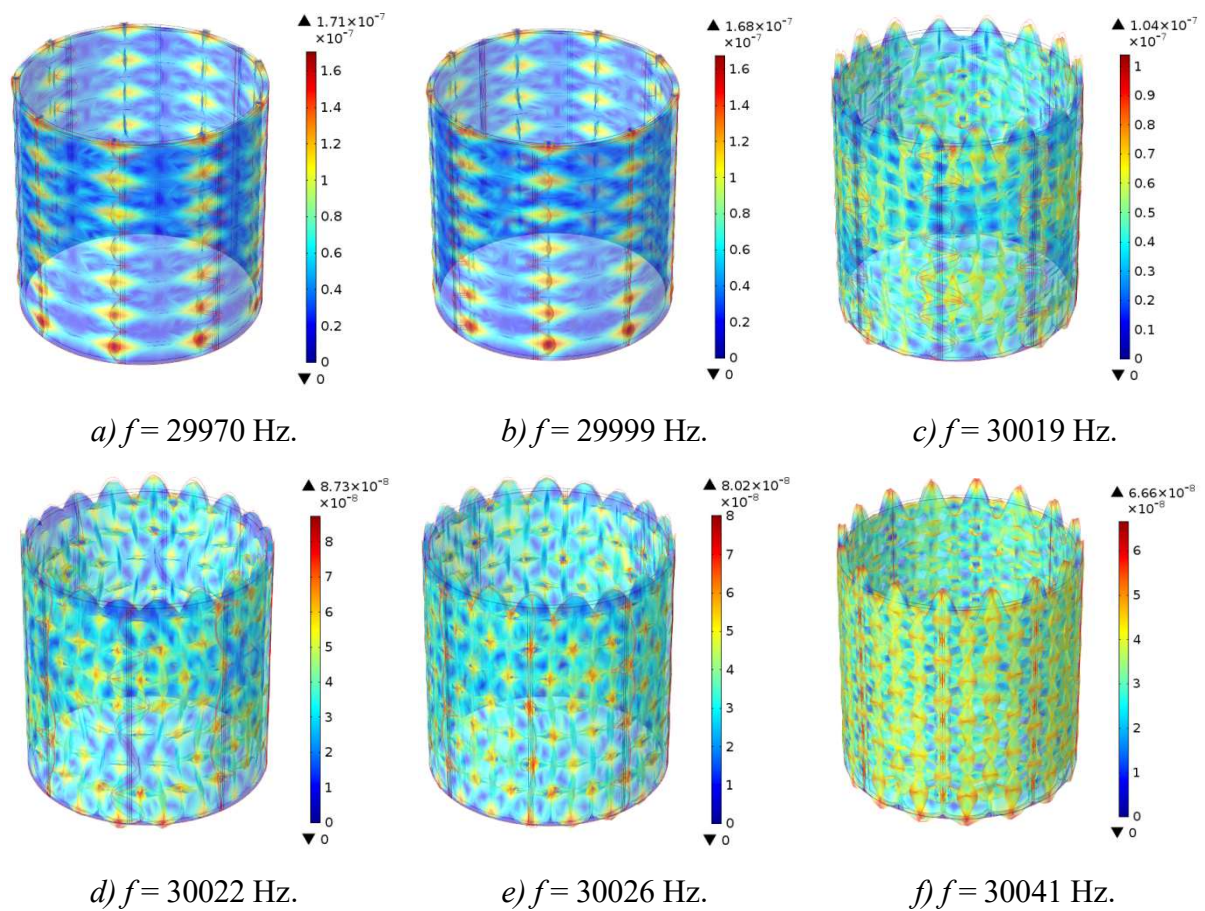


c) $t = 1.237$ ms.

d) $t = 1.24$ ms.

Figure 3.3 PZ tube deformation dynamics, shown in color map.

In order to visualize the own modes of deformation of the piezoelectric cylinder, a modal analysis was performed that allowed the determination of the first 6 own frequencies (damped), structural, of the piezoelectric cylinder and of the associated deformations (Figure 3.4).



a) $f = 29970$ Hz.

b) $f = 29999$ Hz.

c) $f = 30019$ Hz.

d) $f = 30022$ Hz.

e) $f = 30026$ Hz.

f) $f = 30041$ Hz.

Figure 3.4 Modal structural analysis results, first 6 eigenfrequencies.

The modal analysis led to the identification of the own frequencies, around the frequencies of the supply voltage which, in the established electrical and mechanical conditions, present significant deformations.

CHAPTER 4

FLYBACK TRANSFORMER FOR ENVIRONMENTAL ENERGY HARVESTING CONVERTER

The constant increase in demand for unconventional sources, sources that "harvest" environmental energy, has led to the development of small electronic and electromechanical components that capture, convert and possibly store energy from vibration, heat, air currents, light (including ambient light). These devices convert another useful form of energy into useful electricity, energy used to power low-power electronic devices.

A key system used for harvesting ambient energy is the flyback switching source, the main component being the low power transformer with the role of adapting the energy parameters obtained by harvesting to the load requirements.

An unconventional, multilayer hybrid transformer with miniature planar coils is designed to serve the *fly-back* converter for energy harvesting. The magnetic circuit used in the transformer is a hybrid circuit, which contains ferrite and a magnetic nanofluid. If a magnetic nanofluid with 60-70 G is mainly used to improve cooling, the nanofluid with a high concentration of magnetic particles provides 500-1000 G and makes it suitable for inclusion in the magnetic circuit.

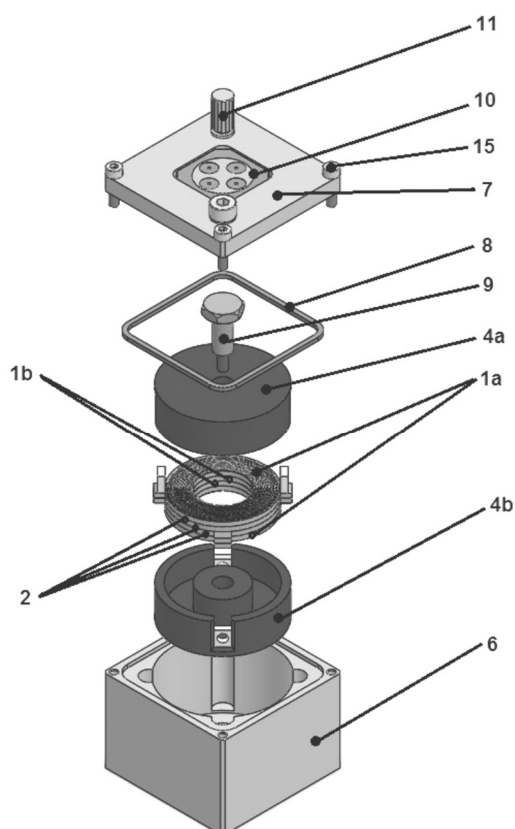


Figure 4.1. Components of the hybrid transformer, with ferrite and magnetic nanofluid.

The transformer with flat coils, miniature, with hybrid magnetic circuit (figure 4.1) contains two flat windings, identical - the primary and the secondary, each consisting of four flat coils, of 20 turns each (1a and 1b), connected in series. The hybrid magnetic circuit consists of ferrite parts

(4a and 4b) and magnetic nanofluid. Ferrite components type 3F3 (4a and b) constitute the solid part of the magnetic circuit.

The fluid part of the magnetic circuit is a magnetic nanofluid with high saturation magnetization (500 - 1000 G), which fills the ferrite housing and bathes the windings of the flat coils. The components are closed in a tank housing (6) by means of the cover, (7), both made of 7075-T6 duralumin alloy, sealed with gasket (8). The center screw (9) secures the ferrite housing with coils. The cover (7) contains the terminals of the primary and secondary winding made on the connection plate (10) and the nanofluid supply system (11). The nanofluid occupies all the available space and contributes to the improvement of the magnetic coupling by eliminating the air gaps, present in the classic transformers and, thus, reduces the magnetic losses. Two types of magnetic nanofluid were used: MNF-UTR-500 and MNF-UTR-1000.

Images during the practical realization of the prototype transformer are presented in figure 4.2.

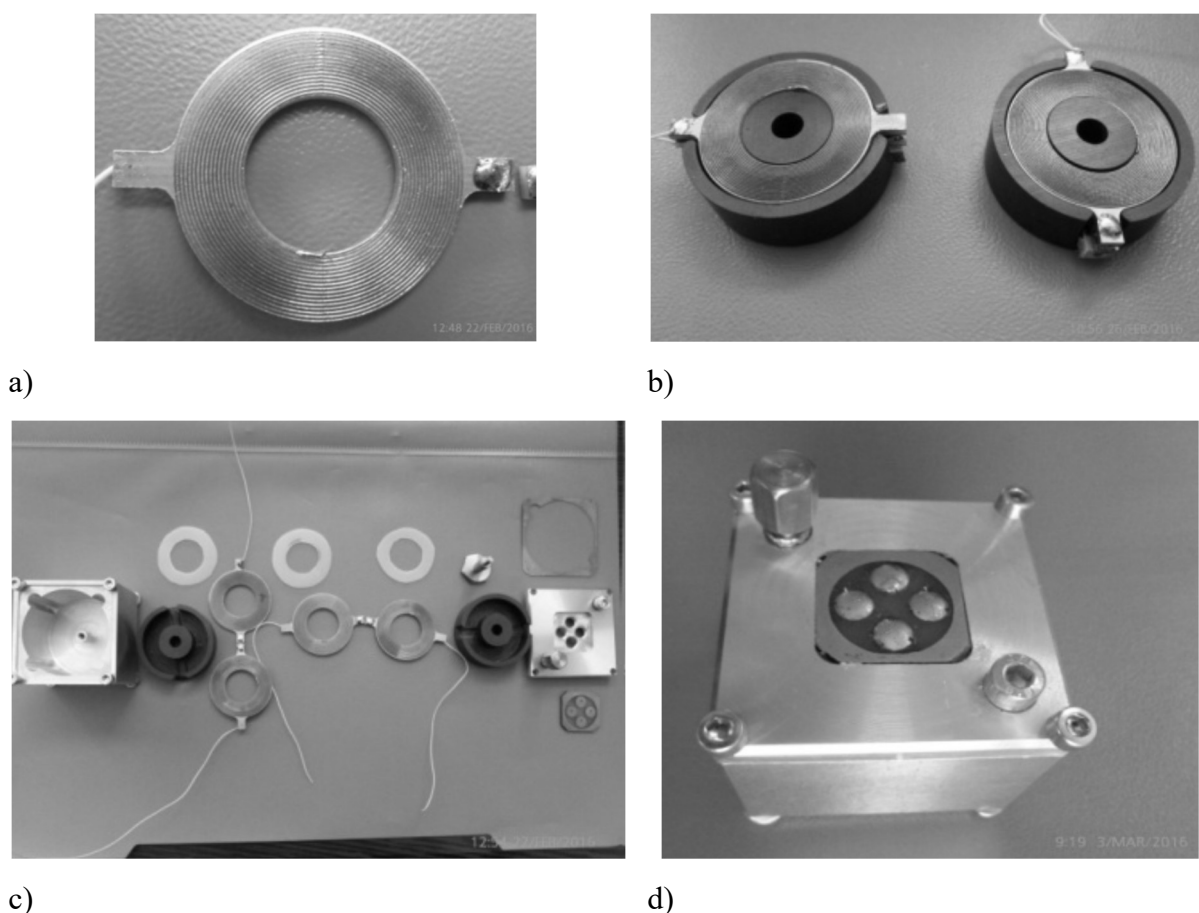


Figure 4.2. Prototype hybrid transformer. (a) flat, spiral coil. (b) coils mounted inside the ferrite core. (c) the constituent elements of the transformer. (d) assembled hybrid transformer.

The windings were shaped like foils, the density of electric current through the coil being replaced with an equivalent surface current density. This simplification affects the calculation of DC resistance.

Numerical simulations were performed using the finite element method. The discretization network was made from approx. 6400000 tetrahedral elements. To reduce the required software / hardware resources, the non-magnetic casing and adjacent elements were not included in the model, the boundary conditions being applied to the outer surface of the ferrite casing.

Figure 4.3 shows magnetic flux density for different equivalent power supply schemes.

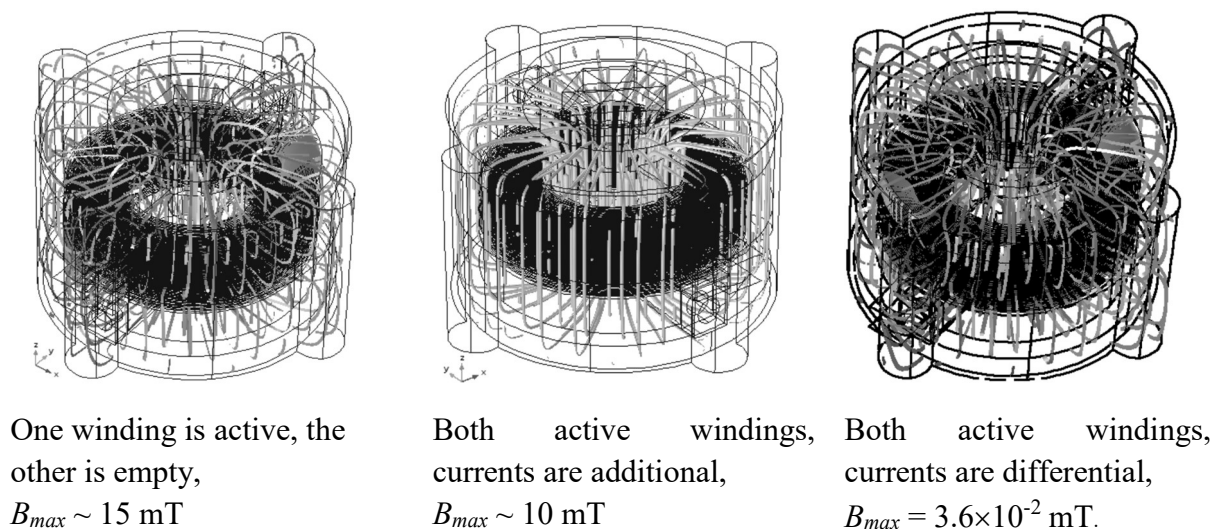
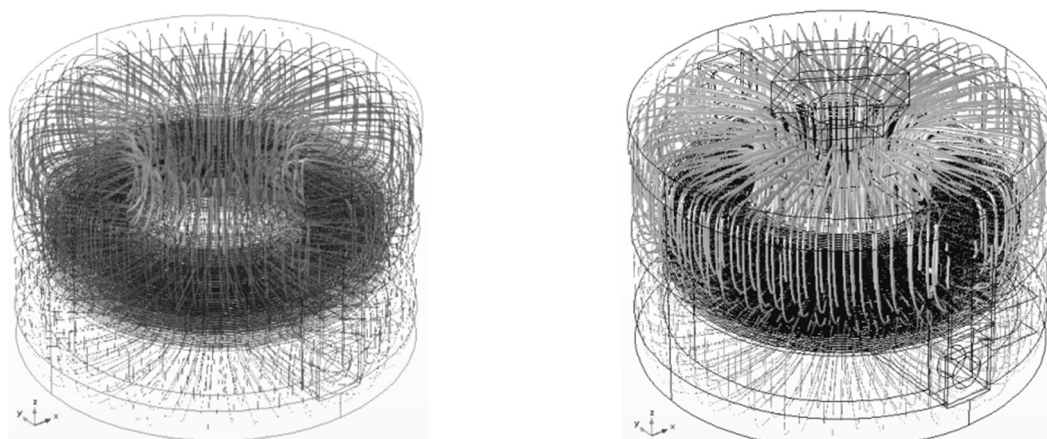


Figure 4.3. Magnetic flux density for several power schemes. Gray levels (light gray: high; dark gray: low) are proportional to local magnitude.

Simulating the behavior of the transformer at 300 kHz, for the two conventional power supply schemes: open circuit (primary on, secondary on empty) and short circuit (primary on, secondary short) we obtain the results from fig. 4.4.



a. Primary on, secondary on empty.

b. Primary on, secondary shorted.

Figure 4.4. Magnetic flux density at 300 kHz, alternating current, through fascicular flux tubes.

The gray level (light gray = large, dark gray = small) and size are proportional to the local magnitude. $B_{max} = 8 \text{ mT}$.

The primary voltage may be lower than the rated voltage specified for the prototype because the electromagnetic media (copper, ferrite, magnetic nanofluid) have linear properties, which ensure the scalability of the results and the invariance of the circuit parameters at the operating frequency.

Under quasi-stationary working conditions, the density of the electric current is unevenly distributed between the coils of the coils, which leads to an increase in the electrical resistance compared to the conditions of direct current.

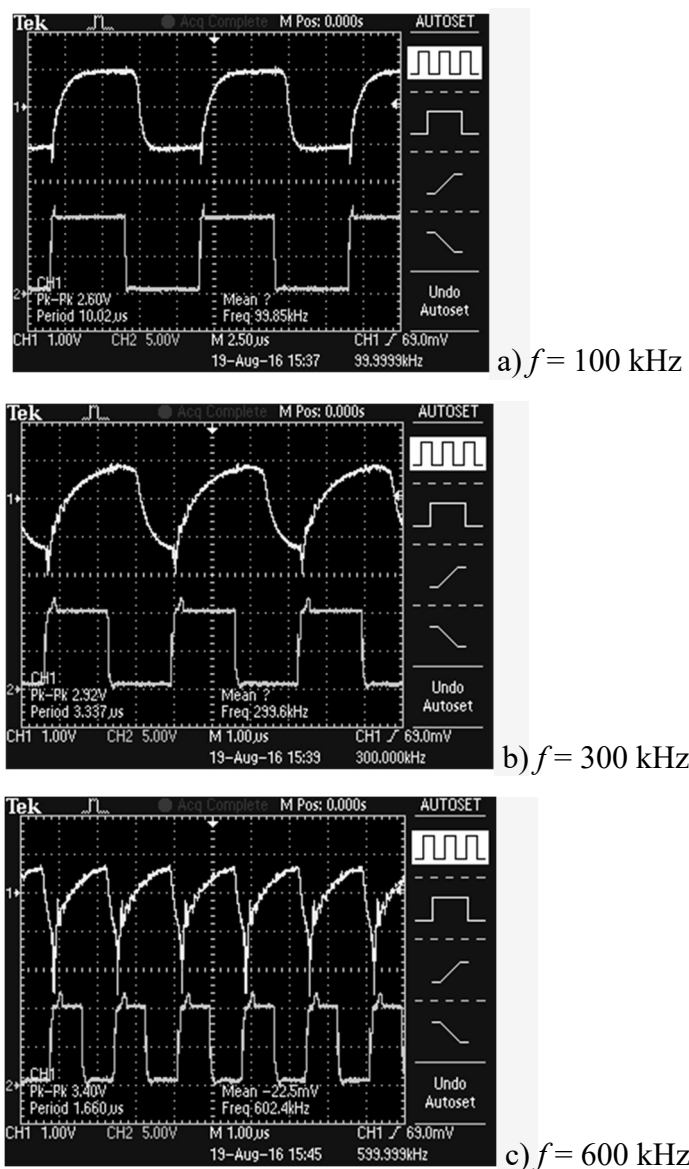


Figure 4.5 Waveforms for the voltage in the secondary winding of the MNF_UTR500 nanofluid transformer (upper curves) and the reference waveforms generated by the signal generator (lower curves).

The waveforms at the output of the secondary winding of the transformer, obtained with a Tektronix TDS 2014B oscilloscope, are shown in Fig. 4.5 a, b, c.

The use of magnetic nanofluids as part of the magnetic circuit in transformers contributes to the improvement of magnetic coupling by eliminating air gaps and therefore to reducing magnetic losses.

The simulations and tests performed on the MNF_UTR500 nanofluid flyback transformer show a suitable behavior for its use in DC / DC converters. The experimental results showed that, using the MNF_UTR500 nanofluid instead of a transformer oil, the quality factors of the primary and secondary windings increase and a better frequency behavior is registered.

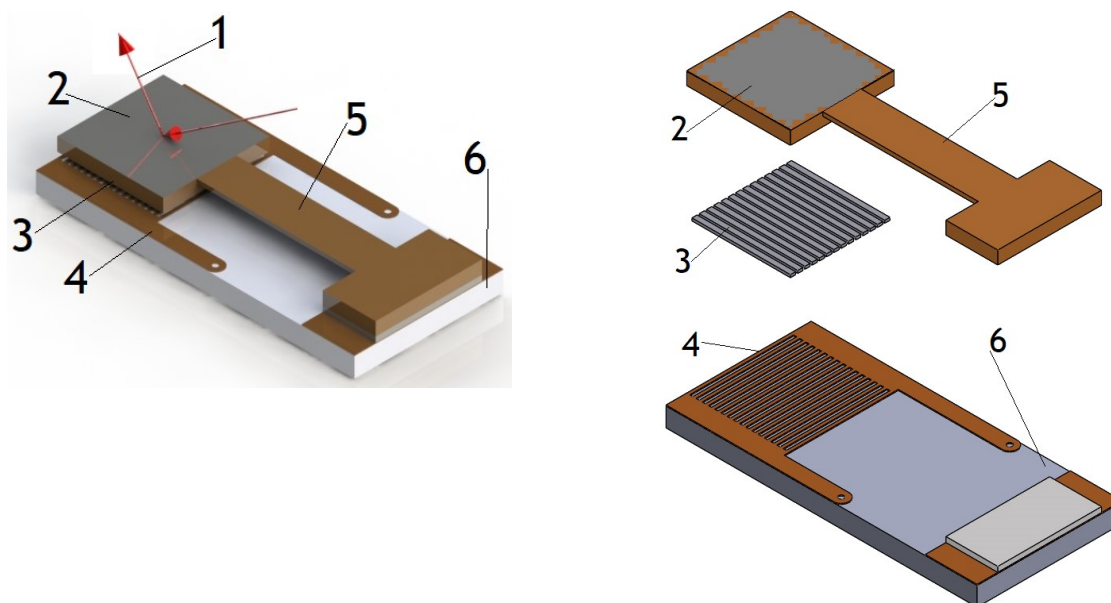
CHAPTER 5

MANUFACTURING TECHNOLOGIES USED TO MAKE ACTUATORS

All the design and simulation efforts for the realization of the actuators cannot be successful without a knowledge and an adaptation to the technological processes that would allow the practical realization of the analyzed devices.

To illustrate the main technological processes that are used for the physical realization of an actuator, I will exemplify with the description of the realization of cantilever electromagnetic microactuators, with beam, which allow the controlled deflection of a laser beam.

The technical solution chosen for this class of actuators is presented in figure 5.1.



Electromagnetic actuator - overview

Electromagnetic actuator - exploded view

Figure 5.1 Electromagnetic actuator with grid with parallel current paths 1- laser beam, 2- mirror surface, 3- micromagnets, 4- grid with parallel current paths, 5-beam, 6- rigid support.

The actuator is composed of a network of permanent magnets (3) integral with the beam (5), which interact with the current paths (4), made on a rigid support (6) on which there is a coupling element.

5.1. Coil and microcoil technologies

The execution of coils and microcoils can be done using several technologies, depending on the desired size, number of turns and number of layers. For classic coils, enameled copper wire is wound on a support spool. For small coils, flat coils are made, in a layer or multilayer, by deposition or removal of conductive material.

The manufacturing process of flat coils using LIGA technology and chemical corrosion

The manufacturing process started from a rigid fiberglass plate (2) (sticlotextolite), covered with a layer of copper (1), which in turn is covered with a thin layer of photoresist (3). The future shape of the current path (flat coil or grid with parallel current paths) was configured in the photoresist layer by exposure to UV radiation.

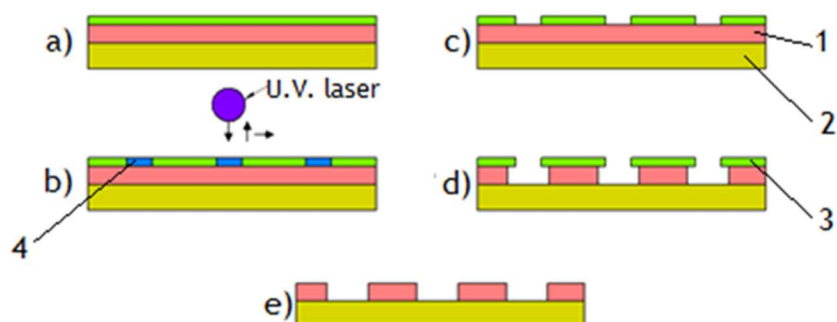


Figure 5.2 The technological process for obtaining flat coils (1- copper layer 35 μm thick; 2- glass-textile plate; 3- thin layer of photoresist, 4- exposed photoresist)

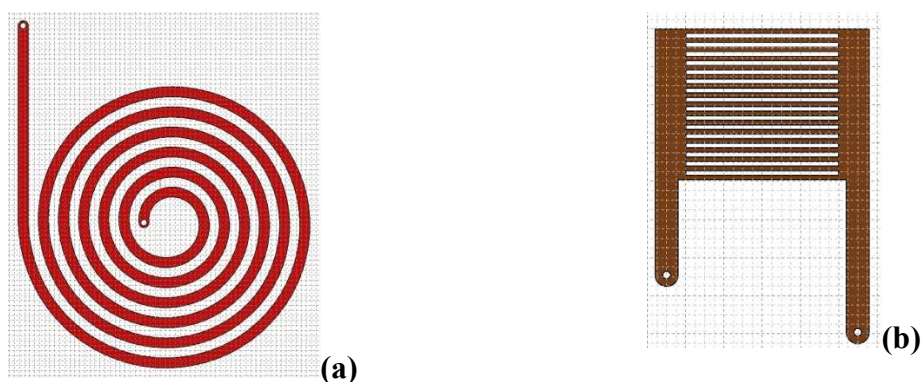


Figure 5.3 Flat coil and grid with parallel current paths - production drawings

Flat coils have the following characteristics: number of turns - 7, thickness of the coil - 0.035 mm, width of the coil - 0.22 mm, distance between turns: 0.22 mm. Current grids with parallel paths have the following characteristics: the number of current paths - 17, the thickness of the coil - 0.035 mm, the width of the coil - 0.12 mm, the distance between the coils - 0.12 mm. The overall dimensions being similar, the structures were made in a matrix of 5x5 elements, resulting in 25 pieces.

The manufacturing process of flat coils using masks and chemical corrosion

Using the same technology, starting from a double-plated copper-plated semi-finished product, coils can be made in two layers, coils with terminals on the second side or coupled coils / transformers. These coils can be made using direct writing or UV exposure masks. Using a double-plated glass-textured substrate, with a thickness of the copper layer of 0.105 mm, coils with 4 and 8 turns were made, as in the figure below (fig. 5.4).

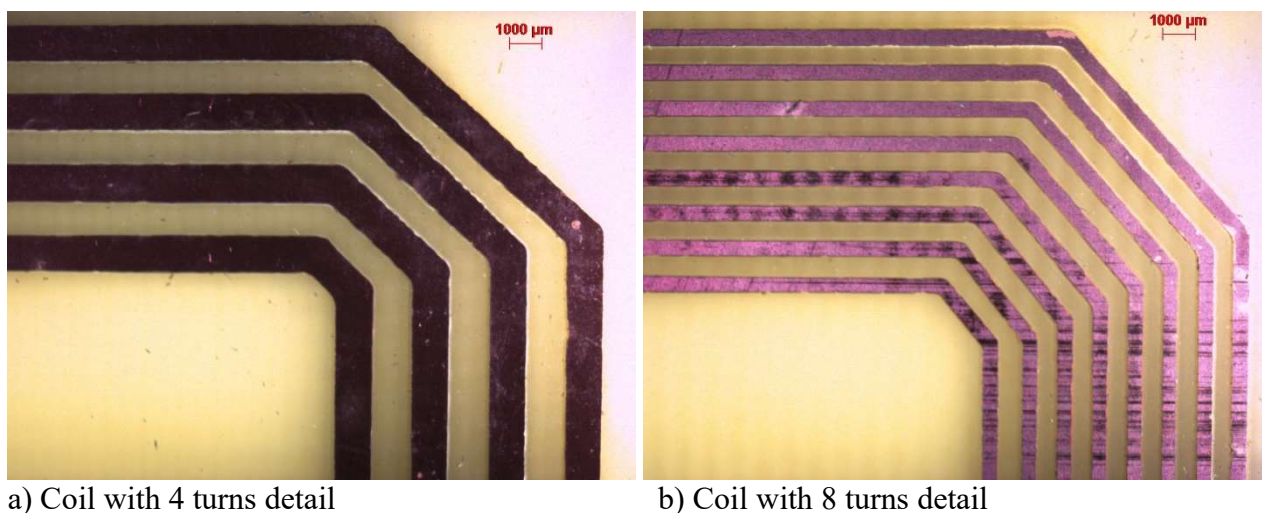


Figure 5.4 Coils with 4 and 8 turns made using masks, 6.5x optical microscopy

Using 2 terminal plates together with 2-coil plates with 4 turns and 2-coil plates with 8 turns each, a transformer structure with flat coils is obtained (primary and secondary, with output connections).

The manufacturing process of multi-layer flat coils

To use more than two coils on a substrate it is necessary to use the technology of making multilayer wiring.

The manufacturing process of flat coils by mechanical processing

An alternative technology to those presented above is mechanical machining on numerically controlled machines, using milling and drilling operations.

The realization of the flat coils started from the single and double copper-plated glass semi-finished product. The coils were obtained by mechanical processing (milling). Details with coils made by this technology are shown in Figure 5.5.

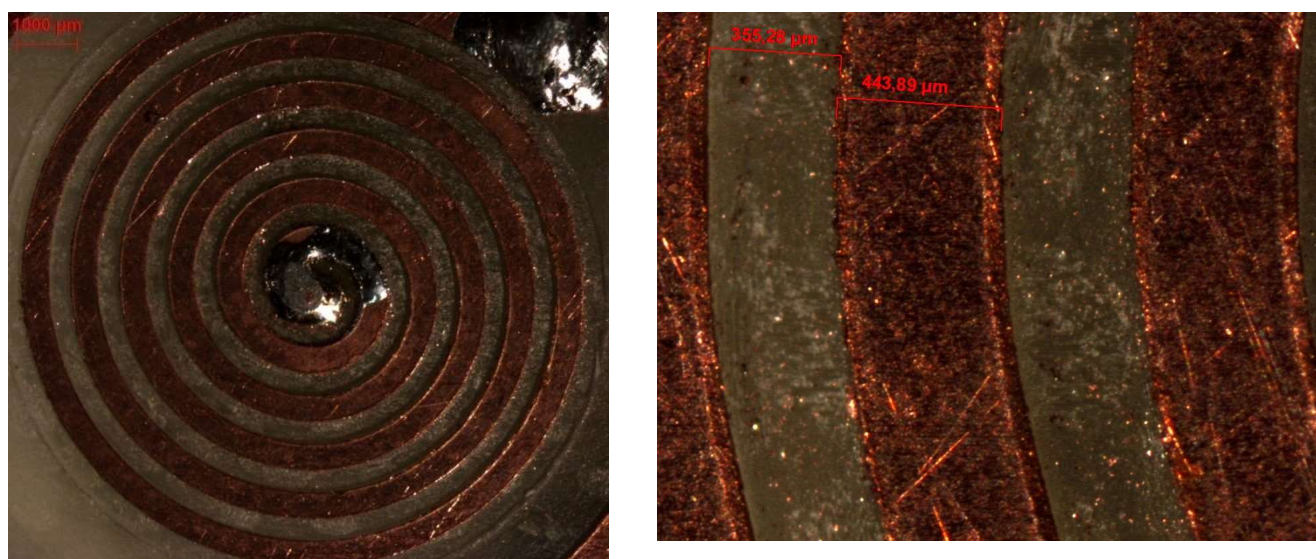


Figure 5.5 Making flat coils by milling

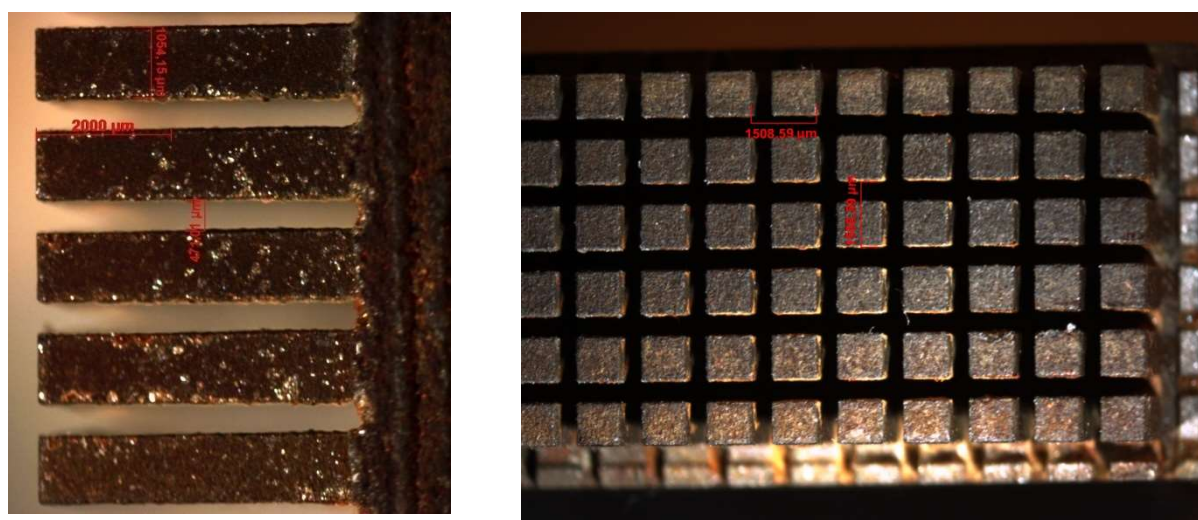
5.2 Permanent magnet processing technologies

The processing of permanent magnets involves making magnets in the designed shape and dimensions and magnetizing them.

Electroerosion processing of permanent magnet matrices

The processing of the matrix with magnets starts from a semi-finished product made of rare earth NdFeB.

The realization of the permanent magnet matrices involved, in a first phase, the realization of a parallelepiped semi-finished product from an NdFeB block. In this semi-finished product, wires with a width of 1 mm, equidistant (the distance between the blades of approximately 0.5 mm) were cut using wire EDM, fig. 5.6.a. The semi-finished product was rotated 90 °, the slats were cut with the same parameters, obtaining a matrix of equidistant pillars - micromagnets, as in fig. 5.14.b. The elastic lamella was glued with resin on the front face of the matrix, the lamella being aligned with the magnet matrix. The micromagnets were cut to the desired height.



a. A blank containing magnets blades matrix, optical microscopy, 12,5x b. A blank containing pillars of the matrix magnets, optical microscopy, 8x

Figure 5.6 Making a matrix of permanent magnets

The magnetization of the permanent magnets was achieved by applying a 1450V pulse for 2 ms on the Helmholtz coil. To concentrate the magnetic field in order to obtain the required magnetization, a dedicated system is used, a field concentrator like the one in figure 5.7.

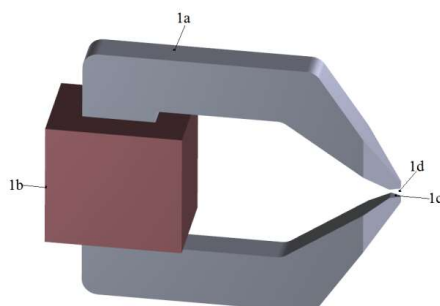


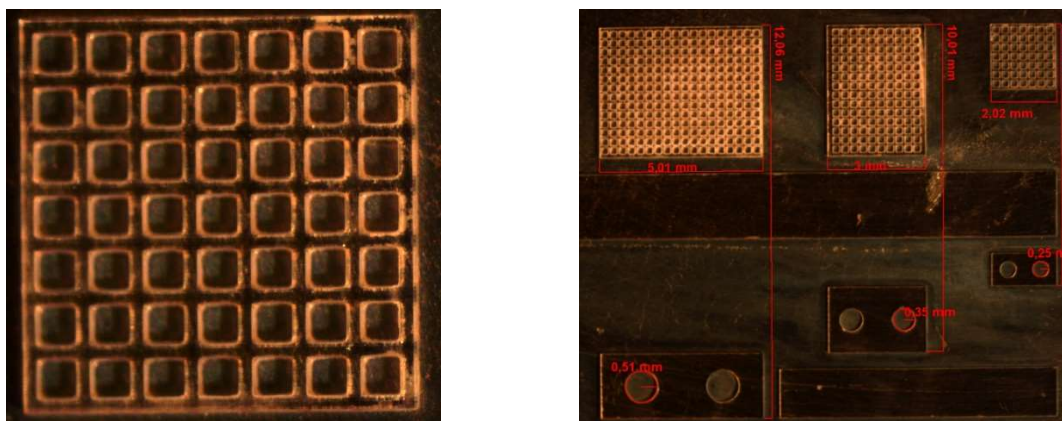
Figure 5.7. Field concentrator, (1a) ferromagnetic core, (1b) coil, (1c) polar soles, (1d) air gap

When applying a high intensity current pulse, the magnetization of the magnet placed in the air gap is obtained.

Electrodeposition of permanent magnet matrices. NiCoMnP deposition in the magnetic field

In order to achieve the electrodeposition in the magnetic field of the micromagnet matrices, we start with the preparation of the support, followed by the realization of the template from SU8 and continuing with the electrodeposition in the magnetic field.

Figure 5.8 shows images with structures during the process for determining the working parameters.

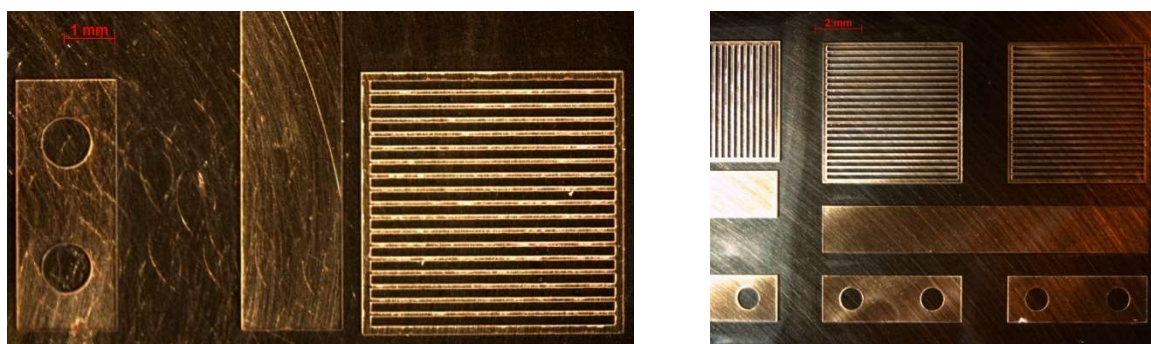


a. Matrix 2 mm x 2 mm, optical microscopy x40

b. SU8 templates for test structures with coupling elements, optical microscopy x6,5

Figure 5.8. Templates for matrix structures

For lamellar structures with a width of 200 μm , spaced at 80 μm , the same technological parameters were used, resulting in structures from figure 5.9.



Lamellar structures 5mm x 5mm, optical microscopy x10

Lamellar structures 4mm x 4mm, optical microscopy x6,5

Figure 5.9. Templates for lamellar structures

For **magnetic field NiCoMnP deposits**, it is necessary to optimize the contents of the baths and the operating conditions by magnetic field electrolysis, in order to obtain the coercivity of NiCoMnP magnetic alloys more than double that obtained by electrodeposition without external magnetic field. The electrolysis tank will be plated with magnetic plates so that the external magnetic field is perpendicular to the surface of the substrate.

Galvanostatic deposition, in which a constant current is applied without potential control, is the commonly used technique for electrodeposition of NiCo-based alloys. The method does not require complex equipment and reference electrodes, using a deposition bath with a standard cathode and a stabilized direct current source.

Thick layers of NiCoMnP of approximately $100\mu\text{m}$ were obtained after a 24h deposition.

After optimizing the parameters, electrodepositions were made in the SU8 photoresistor template, examples with the resulting structures being presented in figure 5.10 (matrix structures) and figure 5.11 (lamellar structures).

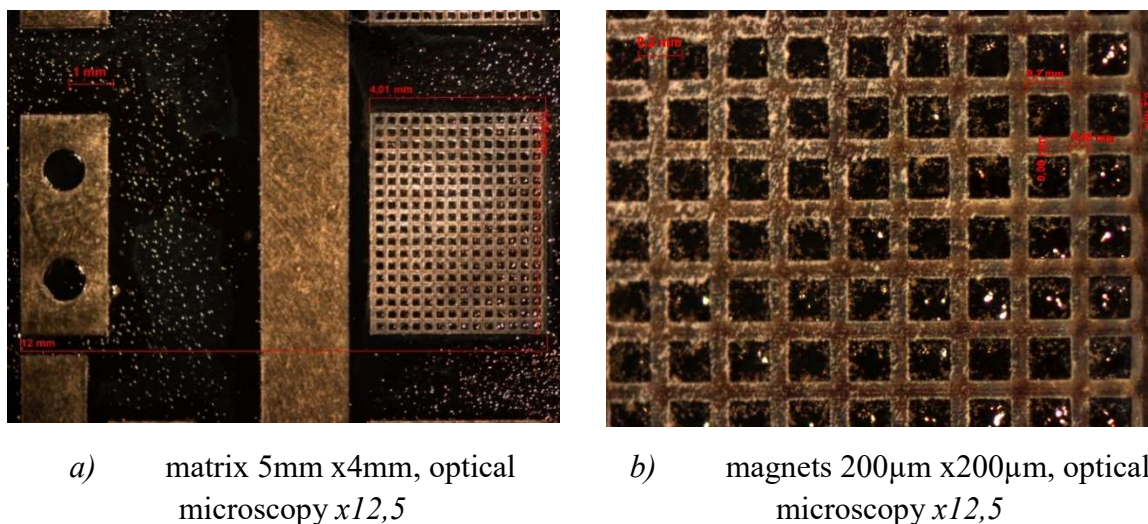


Figure 5.10. Micromagnets in matrix structure

The deposition of NiCoMnP in the magnetic field in the photoresist pattern SU8 was obtained glossy, uniform, inside the pattern, with a few dendrites on the edges.

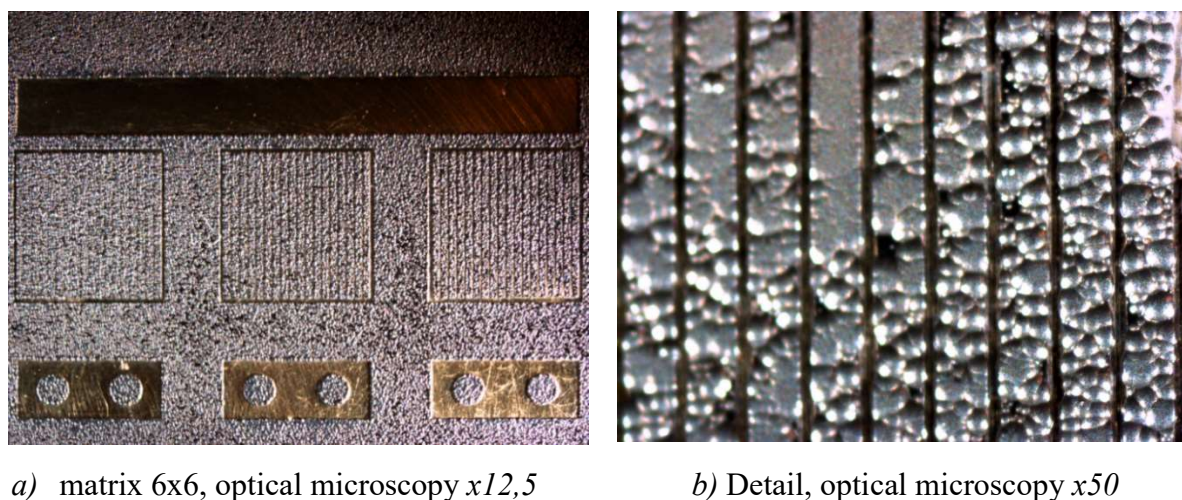


Figure 5.11. Micromagnets in lamellar structure

Electrolytic baths containing cobalt chloride and nickel chloride have high penetration power and stability and have been used for the electrodeposition of nanocrystalline and smooth NiCoMnP films.

5.3. Technologies for making magnetostrictive and piezoelectric actuators

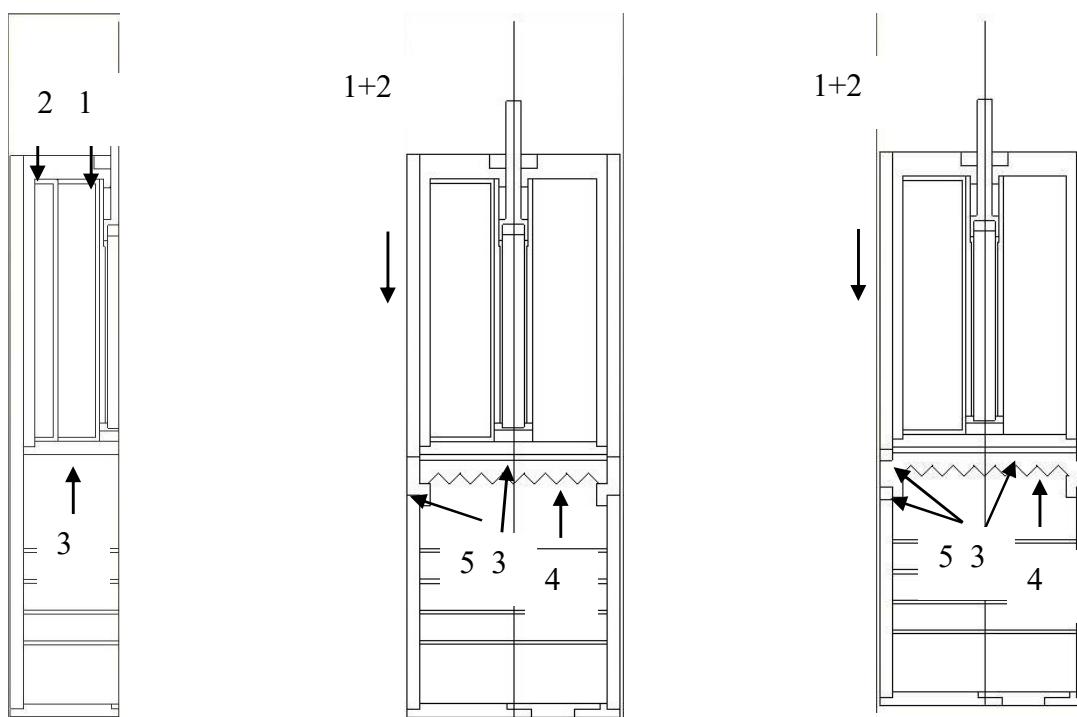
The magnetostrictive linear actuator has been practically made (fig. 5.12).



Figure 5.12 Magnetostrictive linear actuator - practical realization

The realization and testing of the magnetostrictive linear actuator confirmed the theoretical analyzes, the analytical dimensions and the numerical calculations performed, but at the same time data were obtained for the improvement of the constructive solution.

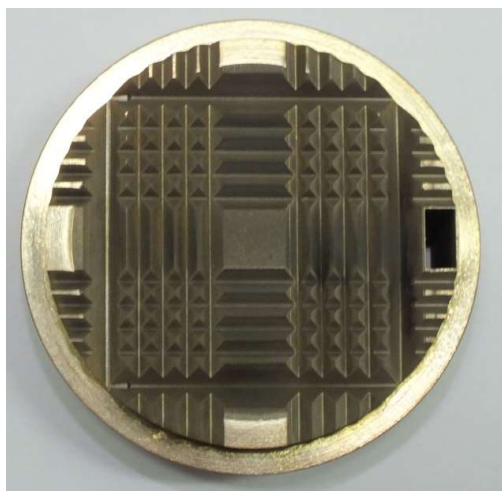
Improvement of the constructive solution was achieved by: making both coils (bias and drive) on a single spool (details in fig. 5.13 b, c), by perforating the spool flanges (upper and lower) and filling these spaces with resin, by making a radiator for heat dissipation to allow the efficient operation of the two possible mechanisms in the absence of a fluid to wash the radiator: conduction and radiation. This radiator was provided with small pyramids to allow the transfer of heat by radiation to the screen surface of the electronic module.



a. initial prototype b. improved prototype - variant A c. improved prototype - variant B

Figure 5.13 Magnetostrictive linear actuator - Initial model and improved variants 1. spool for actuating coil, 2. spool for magnetic bias coil, 1 + 2. spool for both coils (drive and magnetic bias) 3. Peltier element area, 4. radiator, 5. thermal insulation ring

In fig. 5.14 are presented images with the practical achievements of the modified radiator (variant B) and of the coil spool (drive and magnetic bias) with holes for improving heat transfer.



a. Radiator - B variant

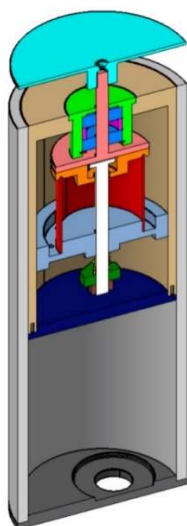


b. Spool with coils - B variant

Figure 5.14 Magnetostrictive linear actuator components – B variant

The realization of a prototype of a rotating piezoelectric motor involved the realization of the component parts using classical technologies (milling, turning, drilling, spinning) and microprocessing (milling and drilling with small tools, operating at high speeds).

Figure 5.15 shows a section through the rotating piezoelectric motor - design (a) and the image of the prototype of the assembled motor (b).



a)



b)

Figure 5.15. Piezoelectric rotary actuator. Section by 3D model (a) and prototype (b)

Figure 5.16 shows the rotor assembly mounted on the stator plate, before the final assembly. The metal components were made by turning, drilling and threading on numerically controlled machines.



a) view from the shaft



b) processing detail

Figure 5.16. Rotor assembly mounted on the stator plate. Processing details of the piezoelectric cylinder.

The piezoelectric cylinder was purchased in the desired dimensions, with a silver coating with a thickness of 35 μm and was divided by mechanical removal of the coating (by microfilling).

5.4. Mechanical parts processing technologies through unconventional technologies

One method of executing mechanical parts for actuators is microprocessing on numerically controlled machine tools, machines that allow processing at high speeds and with small tools. Images during processing and programming are shown in Figure 5.17.



a) Programming structure with double beam



b) Detail of processing the structures

Figure 5.17. Microstructure programming and processing using KERN Micro

An alternative method of realizing the elastic (mobile) structure for the microactuator is the wire EDM processing. Images during the cutting process are shown in Figure 5.18.



Figure 5.18. Cutting test structures using wire EDM

For experiments, two beam widths of 0.75 mm and 0.35 mm were made, some results being presented in fig. 5.19.



12mm x5mm, 0,75mm beams 12mm x5mm, 1,5mm beam 12mm x 6mm, 0,75mm beams

Figure 5.19. Test structures made by EDM with BzBe and stainless steel

The assembly of the console-type electromagnetic micro-actuators (with beam) was done under a microscope. For solenoid coil microactuators, the coil soldering operation has been added to the lower surface of the support plate.

Analyzing the microactuator composed of a fixed lower part (on which the flat coil is located) and a movable upper part (the matrix with permanent magnets and the connecting beam / beams) it was concluded that the two subassemblies pass coupled with each other taking degrees of freedom. A good positioning, which ensures repeatability, can be obtained using precisely made coupling elements and simpler product. The mother-type structures made are those in figure 5.20.

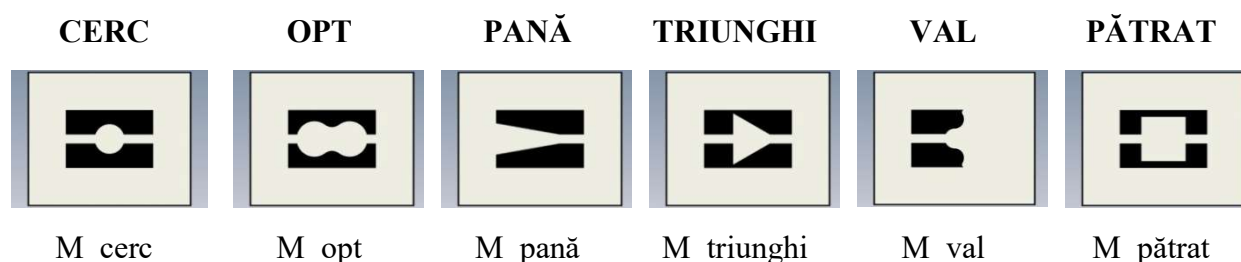


Figure 5.20. Female coupling elements

From the point of view of their functionality we distinguish closed structures, which take over all degrees of freedom from the plane (circle, eight, triangle and square) and open structures, which allow the axial movement of the components (wedge and wave).

The realization of the coupling structures involved the performance of the operations characteristic of LIGA technology. Two-dimensional structures made of SU8 photoresistor (negative) were made. Figure 5.21 shows images with the structures made, after development, drying and post-exposure baking.

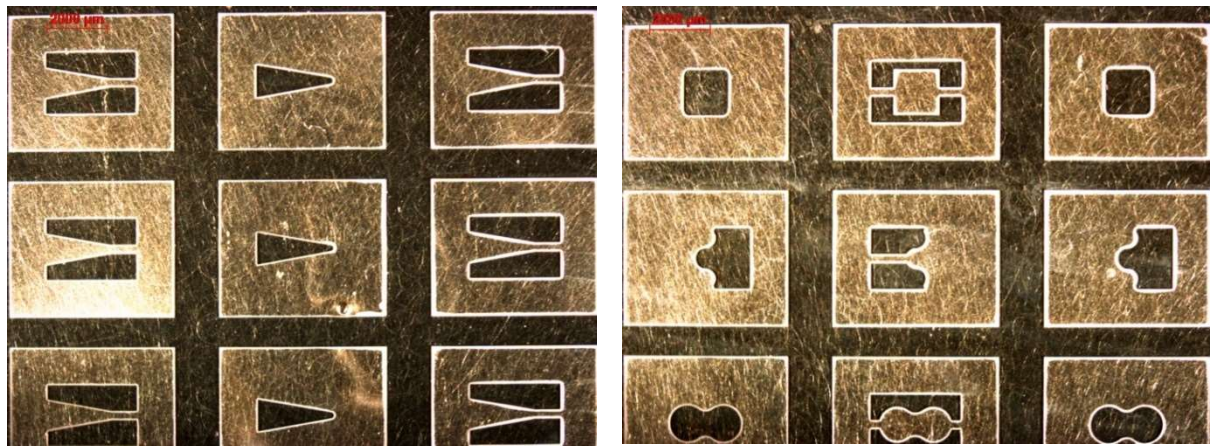
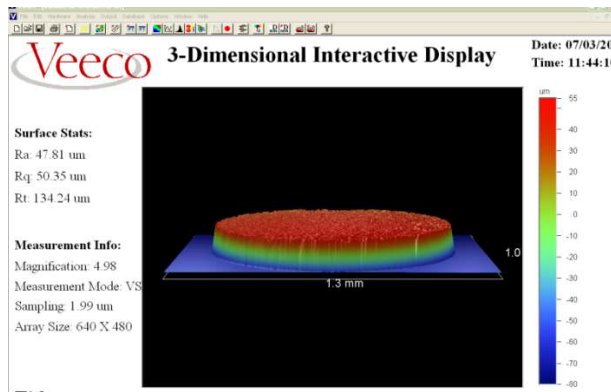
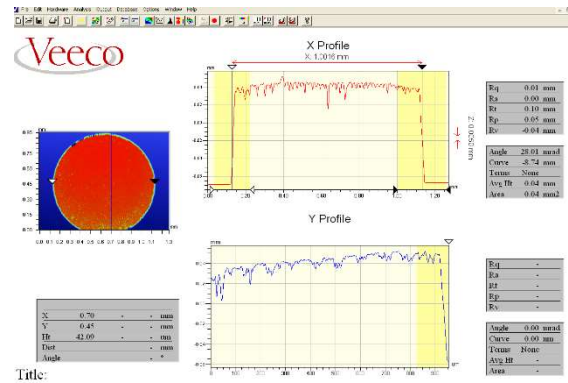


Figure 5.21. Assembly structures, template made of photoresist SU8

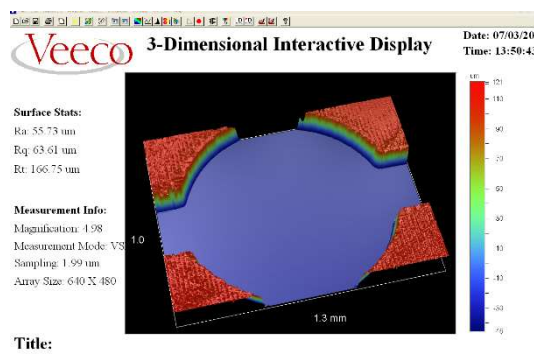
To determine the quality and accuracy of the assembly structures, comparative measurements of the mother-father structures were made, using the Veeco interferometer, as in figure 5.22.



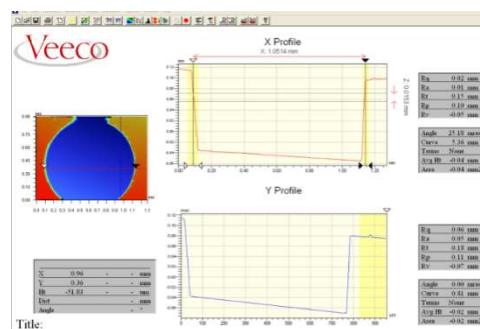
3D structure, male circle



Determination of the diameter for the male ring coupling element



3D structure, female circle



Determination of the diameter for the female ring coupling element

Figure 5.22. Measurements of coupling structures by interferometry

After determinations, a good correlation between dimensions is observed, resulting in a gap below 0.2 μm .

CONCLUSIONS, CONTRIBUTIONS, PROSPECTS

Thesis entitled "*Interaction electromechanical sizing and construction of drive systems with integration micro electromechanical*" deals interactions electromechanical a series of drives containing elements of micro electromechanical, presenting variants have been analyzed in the simulations with the technological solutions adopted, with the practical achievements and with the tests performed for the validation of the solutions.

The first chapter of the paper analyzes some variants of magnetostrictive actuators. After a general analysis of magnetostrictive materials with practical applications, the magnetostrictive material commercially known as Terfenol-D was identified and analyzed. one or two cylindrical coils. The variants validated following the simulations were practically executed, tested and improved. Constitutional optimizations of the model were performed regarding the shape factor of the magnetostrictive material rod and the magnetostrictive material / permanent magnet ratio for an imposed volume. The electronic blocks necessary for the command and control of the actuator were practically made and tests were made for the practical determination of the characteristics of the actuator, resulting in the possibility of its use in the aerospace field. The identified solutions are original, they being included in the patent application A / 00879 / 17.11.2014 "Magnetostrictive linear motor".

The second chapter of the thesis presents electromechanical actuators based on interactions between magnetic materials and electromagnetic coils. Several constructive solutions were identified and the electromechanical beam type console actuators were studied. Structural deformations were determined for the own structural modes, using reduced models due to symmetry and complete models.

The third chapter of the thesis presents the piezoelectric actuators. The appropriate mathematical model was identified and the deformation of a piezoelectric cylinder was determined, analyzing the structural deformations and deformations associated with the stator's own modes. The identified solutions are original, they are included in the patent application A / 00874 / 23.11.2015 "Rotary piezoelectric motor with double contact".

The fourth chapter is dedicated to the study of a flyback transformer for an environmental energy converter. A constructive solution of hybrid transformer is identified, with ferrite and magnetic nanofluid. For this constructive variant starting from the mathematical model, the operation was simulated using numerical methods, the necessary technological processes were identified and practically such a transformer was realized, which was tested for validation. Simulations and tests performed on the transformer flyback with nanofluid MNF_UTR500 show a suitable behavior for its use in DC / DC converters. The identified solutions are original, they are included in patent application A / 00713, 07.10.2016.

The fifth chapter identifies, customizes and describes the main technological processes involved in the practical realization of the studied actuators. The manufacturing technologies of coils and microboils were analyzed, in a single layer and multilayer and practically several constructive variants were made. The technologies for processing permanent magnets, by EDM and by magnetic field deposition, have been identified, customized and practically used. These technologies having applicability mainly to electromagnetic actuators, their quasi-static testing was performed. For the realization of magnetostrictive and piezoelectric actuators,

unconventional technologies have been identified and customized for concrete applications. Practically two variants of linear magnetostrictive actuator and a variant of rotating piezoelectric actuator were made. Because it is a common element of many actuating elements, a family of coupling elements applicable in the field of microsystems was made and verified.

Author's original contributions in the field of electrical engineering on the issues addressed are:

- ❖ Documentary study on the current state and comparative analysis regarding the magnetostrictive materials, with the detailing of the Terfenol-D material,
- ❖ Documentary study on linear magnetostrictive actuators,
- ❖ Conception and dimensioning of a magnetostrictive actuator with planar coils and study on it, mainly by numerical modeling,
- ❖ Conception of magnetostrictive actuator with cylindrical coils and study on it, mainly by numerical modeling,
- ❖ Study on the constructive optimization of the magnetostrictive actuator, mainly by numerical modeling,
- ❖ Variant conception of console type electromagnetic actuator, with study on the technologies of practical realization and on the deformations for the own structural modes by numerical modeling,
- ❖ Study on the deformation dynamics of a piezoelectric rotor, mainly by numerical modeling,
- ❖ Technical solution and study on the technologies for the practical realization of a hybrid transformer, with ferrite and magnetic nanofluid,
- ❖ Technical solution for making coils and microbools, ⌘ Technical solution for making the matrices of permanent magnets by EDM and the template for making the matrices by deposition,
- ❖ Technical solution for achieving cooling and improving heat transfer for the magnetostrictive actuator,
- ❖ Technical solution for achieving the division of the active piezoelectric cylinder,
- ❖ Participation in the identification of patentable elements for three patent proposals,
- ❖ Participation in the dissemination of research results by publishing in the volumes of conferences and in specialized journals indexed in international databases, some listed ISI,
- ❖ Participation in the dissemination of knowledge on production technologies for small components by publishing a book.

Considering the interest for the study of electromechanical interactions in a series of drive systems containing microelectromechanical elements, the development perspectives are numerous, among the most important being:

- ❖ Miniaturization of the magnetostrictive linear actuator,
- ❖ Integration of the command and control system of the magnetostrictive actuator, ⌘ Extending the modeling of the linear magnetostrictive actuator to model the thermal behavior in terrestrial and aerospace applications,
- ❖ Development of a feedback loop control system for the console type electromagnetic actuator,

- ❖ Miniaturization of the piezoelectric rotary actuator, especially in terms of command and control blocks,
- ❖ Development and integration in a single system, made using microelectromechanical manufacturing technologies, of the hybrid transformer to obtain a miniature system for converting the energy collected from the environment. Dezvoltarea și integrarea într-un singur sistem, realizat utilizând tehnologii de fabricație microelectromecanice, a transformatorului hibrid pentru a obține un sistem miniatural de conversie a energiei recoltate din mediul ambiant.

REFERENCES

- [1] C. Ilie, **M. Popa**, N. Tănase, *Componente și sisteme micromecanice fabricate prin tehnologia LIGA*, Editura ELECTRA, București, 2020, ISBN 978-606-507-127-8.
- [2] **M. Popa**, A. M. Morega, L. PÎSLARU-DĂNESCU *Microactuator magnetostrictiv*, Simpozionul de Mașini Electrice SME '15, 2013, Universitatea Politehnica din București, CD Proceedings, pg. 1-6, ISSN: 1843-5912
- [3] .:, *Noi tipuri de actuatori specifici aplicațiilor spațiale - ACTOSPACE*, Contract 88/2013 - Raport științific și tehnic,
- [4] **M. Popa**, A. M. Morega, Mihaela MOREGA, *Optimizarea unui actuator magnetostrictiv*, Simpozionul de Mașini Electrice SME '14, 2014, Universitatea Politehnica din București, CD Proceedings, pg. 1-7, ISSN: 1843-5912
- [5] L. Pîslaru-Dănescu, A.M. Morega, M. Morega, F. Bunea, **M. Popa**, C. A. Băbuțanu, *A new type of linear magnetostrictive motor*, Springer Electr. Eng (2017) 99:601-613,
- [6] **M. Popa**, A.M. Morega, L. PÎSLARU-DĂNESCU, M. MOREGA, *Actuator magnetostrictiv - o analiză bidimensională*, Simpozionul de Mașini Electrice SME '16, 2016, Universitatea Politehnica din București, CD Proceedings, pg. 1-7, ISSN: 1843-5912
- [7] Y. Veli, A.M. Morega, L. Pislaru-Danescu, M. Morega, **M. Popa**, *Studiul unui motor cu magnetostricțiune liniar*, Simpozionul de Mașini Electrice, SME '19, ediția a XVa, 15 Noiembrie, 2019, Facultatea de Inginerie Electrică, UPB, ASTR, IEEE-Romania, ISSN, ISSN-L: 843-5912.
- [8] L. Pîslaru-Dănescu, A. M. Morega, M. Morega, R Chihaiia, **M. Popa** and L. Flore, *Electronic Drive System of a Linear Magnetostrictive Motor Designed for Outer Space Applications* THE 9TH INTERNATIONAL SYMPOSIUM ON ADVANCED TOPICS IN ELECTRICAL ENGINEERING (ATEE), 2015., 978-1-4799-7514-3/15/\$31.00
- [9] A. M. Morega, N. Tănase, **M. Popa**, M. Morega and J. B. Dumitru, *Numerical simulation of an electromagnetic bending-mode cantilever microactuator*, 2013 8TH INTERNATIONAL SYMPOSIUM ON ADVANCED TOPICS IN ELECTRICAL ENGINEERING (ATEE), 2013, pp. 1-6, doi: 10.1109/ATEE.2013.6563478.
- [10] .:, *Actuatori electromagnetici și electrodinamici procesați prin tehnologie LIGA*, Contract 249/2014, Raport științific și tehnic
- [11] A.M. Morega, G. Robello, M. Morega, L. Pîslaru-Dănescu, *Numerical Study of the Stator Motion in a Piezoelectric Ultrasonic Motor*, *The 9th International Symposium on Advanced Topics in Electrical Engineering*, May 7-9, 2015, Bucharest, Romania.
- [12] A. M. Morega, M. Morega, L. Pîslaru-Dănescu, **M. Popa** *Simularea funcționării rotorului unui motor piezoelectric cu undă călătoare*, Simpozionul de mașini electrice SME '15 – 23 Octombrie, 2015
- [13] L. Pîslaru-Dănescu¹, A. M. Morega, J. B. Dumitru, M. Morega, N. C. Popa, F. D. Stoian, D. Susan-Resiga, S. Holotescu, **M. Popa**- *Miniature Planar Spiral Transformer with Hybrid, Ferrite and Magnetic Nanofluid Core*, IEEE Transactions on Magnetics – 4600614, october 2018, volume 54, number 10, ISSN 0018-9464

- [14] .:, *Componente și sisteme microelectromecanice (MEMS) realizate prin tehnologii specifice cu aplicații în medicină, microfluidică și în realizarea de micromotoare și microactuatori - TSMEMS*, Contract Nucleu 09350101/2009, Raport științific și tehnic
- [15] C. Ilie, **M. Popa**, P. Prioteasa, I. Chiriță, N. Tănase, *Application of LIGA Technology for the Development of Micromechanical Systems*, U.P.B. Sci. Bull., Series D, Vol. 73, Iss. 2, 2011, Bucuresti, ROMANIA, ISSN 1454-2358
- [16] C. Ilie, **M. Popa**, P. Prioteasa, I. Chiriță, N. Tănase, *Application of LIGA Technology for the Development of Micromechanical Systems*, U.P.B. Sci. Bull., Series D, Vol. 73, Iss. 2, 2011, Bucuresti, ROMANIA, ISSN 1454-2358
- [17] P. Barbu; M.M. Codescu, M Iordoc, V. Marinescu, E. Manta, C. Ilie, **M. Popa**, *Electrodeposition of CoNiMnP Thick Films for Micromachined Magnetic Device Applications*, REVISTA DE CHIMIE, Volume: 69 Issue: 6 Pages: 1355-1362, Published: JUN 2018
- [18] F.T. Tănăsescu, Ghe. Ștefănescu, C. Ilie, **M. Popa**, S. Dumitru, *Încercări de performanță pentru caracterizarea unui dispozitiv MEMS*, Buletinul AGIR nr. 4/2015 oct.-dec. pag. 97-102
- [19] L. Pîslaru-Dănescu, **M. Popa**, F. Bunea, A.M. Morega, M. Morega, D. Gabor, L. Flore, I. Popescu *Motor liniar magnetostriktiv*. Cerere de brevet A/00879/17.11.2014
- [20] C. Ilie, C.D. Comeaga, O. Dontu, **M. Popa**, *Micro Parts Errors to Precision Manufacturing using UV-LIGA Technology* Advanced Materials Research Vols. 816-817 (2013) pp 237-241
- [21] **M. Popa**, C. Ilie, D. Lipcinski, I. Chirita, N. Tănase, S. Apostol (2018) *Coupling and Assembly Elements Using Microfabrication Technologies*. In: Gheorghe G. (eds) Proceedings of the International Conference of Mechatronics and Cyber-MixMechatronics - 2017. ICOMECYME 2017. Lecture Notes in Networks and Systems, vol 20. Springer
- [22] Pîslaru-Dănescu Lucian, **Popa Marius**, Băbuțanu Corina-Alice, Chihaiia Rareș-Andrei, Morega Alexandru-Mihail, Morega Mihaela, Fuiorea Ion, Flore Lică, Gabor Dumitrița, *Motor piezoelectric rotativ cu dublu contact*. Cerere de brevet: A/00874/23.11.2015
- [23] Pîslaru-Dănescu Lucian, **Popa Marius**, Ilie Cristinel Ioan, Chihaiia Rareș-Andrei, Băbuțanu Corina-Alice, Nicolaie Sergiu, Bunea Florentina, Stoian Floriana Daniela, Holotescu Sorin, Marinică Oana-Maria, Morega Alexandru-Mihail, Morega Mihaela, Dumitru Jean-Bogdan, Popa Nicolae-Călin. *Transformator planar cu nanofluid magnetic* Cerere de brevet: A/00713, 07.10.2016.